



# Laser Doppler Velocimeter Application in Supersonic Boundary-Layer Flow

J. C. Donaldson  
Calspan Corporation

March 1987

Final Report for Period October 1, 1984 — September 30, 1986

Approved for public release; distribution is unlimited.

**TECHNICAL REPORTS**  
**FILE COPY**

PROPERTY OF U.S. AIR FORCE  
AEDC TECHNICAL LIBRARY

**ARNOLD ENGINEERING DEVELOPMENT CENTER**  
**ARNOLD AIR FORCE STATION, TENNESSEE**  
**AIR FORCE SYSTEMS COMMAND**  
**UNITED STATES AIR FORCE**

## NOTICES

When U. S. Government drawings, specifications, or other data are used for any purpose other than a definitely related Government procurement operation, the Government thereby incurs no responsibility nor any obligation whatsoever, and the fact that the Government may have formulated, furnished, or in any way supplied the said drawings, specifications, or other data, is not to be regarded by implication or otherwise, or in any manner licensing the holder or any other person or corporation, or conveying any rights or permission to manufacture, use, or sell any patented invention that may in any way be related thereto.

Qualified users may obtain copies of this report from the Defense Technical Information Center.

References to named commercial products in this report are not to be considered in any sense as an endorsement of the product by the United States Air Force or the Government.

This report has been reviewed by the Office of Public Affairs (PA) and is releasable to the National Technical Information Service (NTIS). At NTIS, it will be available to the general public, including foreign nations.

## APPROVAL STATEMENT

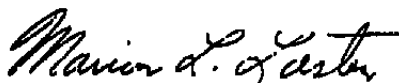
This report has been reviewed and approved.



MALCOLM B. GIVINS, Major, CF  
Facility Technology Division  
Directorate of Technology  
Deputy for Operations

Approved for publication:

FOR THE COMMANDER



MARION L. LASTER  
Director of Technology  
Deputy for Operations

UNCLASSIFIED

SECURITY CLASSIFICATION OF THIS PAGE

## REPORT DOCUMENTATION PAGE

1a. REPORT SECURITY CLASSIFICATION		1b. RESTRICTIVE MARKINGS	
2a. SECURITY CLASSIFICATION AUTHORITY UNCLASSIFIED		3. DISTRIBUTION/AVAILABILITY OF REPORT Approved for public release; distribution is unlimited.	
2b. DECLASSIFICATION/DOWNGRADING SCHEDULE		5. MONITORING ORGANIZATION REPORT NUMBER(S)	
4. PERFORMING ORGANIZATION REPORT NUMBER(S) AEDC-TR-86-44		7a. NAME OF MONITORING ORGANIZATION	
6a. NAME OF PERFORMING ORGANIZATION Arnold Engineering Development Center	6b. OFFICE SYMBOL (If applicable) DOT	7b. ADDRESS (City, State and ZIP Code)	
8a. NAME OF FUNDING/SPONSORING ORGANIZATION Arnold Engineering Development Center		8. PROCUREMENT INSTRUMENT IDENTIFICATION NUMBER	
8b. ADDRESS (City, State and ZIP Code) Air Force Systems Command Arnold Air Force Station, TN 37389-5000		10. SOURCE OF FUNDING NOS.	
11. TITLE (Include Security Classification) SEE REVERSE OF THIS PAGE		PROGRAM ELEMENT NO. 65807F	PROJECT NO.
		TASK NO.	WORK UNIT NO.
12. PERSONAL AUTHOR(S) Donaldson, J. C., Calspan Corporation, AEDC Division			
13a. TYPE OF REPORT Final	13b. TIME COVERED FROM 10/1/84 TO 9/30/86	14. DATE OF REPORT (Yr., Mo., Day) March 1987	15. PAGE COUNT 59
16. SUPPLEMENTARY NOTATION Available in Defense Technical Information Center (DTIC).			
17. COBALT CODES		18. SUBJECT TERMS (Continue on reverse if necessary and identify by block number)	
FIELD	GROUP	SUB. GR.	
20	04	particle dynamics	
20	08	laser Doppler velocimeter	
		boundary-layer flow	
		supersonic flow (cont)	
19. ABSTRACT (Continue on reverse if necessary and identify by block number) Laser Doppler velocimeter techniques have been investigated for nonintrusive measurements of cone boundary-layer mean-velocity profiles in supersonic flow. The investigation was performed in the AEDC Supersonic Wind Tunnel (A) at a free-stream Mach number of 4, using olive-oil droplets to seed the tunnel flow. The basis for the evaluation of the LDV results was a set of velocity profiles obtained using conventional probing techniques. Laminar, transitional, and turbulent boundary layers on a 7-deg (half-angle) sharp-cone model were included in this study. The results obtained in this investigation demonstrate that mean-velocity profiles can be obtained within acceptable limits of uncertainty provided (1) seed particles of appropriate size are found in the tunnel flow or can be added to the flow and (2) a systematic editing procedure is available, when the results are evaluated, to eliminate velocities of relatively low probability and effects of spurious noise.			
20. DISTRIBUTION/AVAILABILITY OF ABSTRACT UNCLASSIFIED/UNLIMITED <input type="checkbox"/> SAME AS RPT. <input checked="" type="checkbox"/> DTIC USERS <input type="checkbox"/>		21. ABSTRACT SECURITY CLASSIFICATION UNCLASSIFIED	
22a. NAME OF RESPONSIBLE INDIVIDUAL W. O. Cole		22b. TELEPHONE NUMBER (Include Area Code) (615) 454-7813	22c. OFFICE SYMBOL DOS

UNCLASSIFIED

SECURITY CLASSIFICATION OF THIS PAGE

11. TITLE

Laser Doppler Velocimeter Application in Supersonic Boundary-Layer Flow

18. SUBJECT TERMS (Concluded)

gas flow measurements  
forward-scattered light

wind tunnel tests  
back-scattered light

UNCLASSIFIED

SECURITY CLASSIFICATION OF THIS PAGE

## **PREFACE**

The work reported herein was performed by the Arnold Engineering Development Center (AEDC), Air Force Systems Command (AFSC) at the request of the AEDC Directorate of Technology (DOT). The AEDC/DOT Project Managers were M. K. Kingery, R. H. Nichols, and Major M. E. Givins. The results were obtained by Calspan Corporation, AEDC Division, operating contractor for the aerospace flight dynamics testing efforts at the AEDC, AFSC, Arnold Air Force Station, Tennessee. The work was performed during the period from October 1, 1984, to September 30, 1985, under AEDC Project Number D283VW (Calspan Project Number V32N-B37) and during the period from October 1, 1985, to September 30, 1986, under AEDC Project Number DB98VW (Calspan Project Number V32B-CE3). The manuscript was submitted for publication October 31, 1986.

The author acknowledges that he has been the beneficiary of the efforts of many coworkers in preparation of the subject matter of this report, but principally F. L. Crosswy who supervised the acquisition of the LDV measurements, F. L. Heltsley who edited the LDV data, and R. H. Nichols who made the theoretical calculations related to particle dynamics. This report has been improved as a result of suggestions offered by each of these coworkers.

## CONTENTS

	Page
1.0 INTRODUCTION .....	7
2.0 APPARATUS	
2.1 Test Facility .....	8
2.2 Test Article .....	8
2.3 Boundary-Layer Survey Mechanism .....	9
2.4 Boundary-Layer Survey Probes .....	10
2.5 Laser Doppler Velocimeter Measurement System .....	10
2.6 Laser Doppler Velocimeter Traversing System .....	11
2.7 Tunnel Flow Seeding Techniques .....	12
3.0 RESULTS AND DISCUSSION	
3.1 Conventional Techniques .....	14
3.2 Seeding of the Flow .....	15
3.3 Simultaneous Component Measurements .....	16
3.4 Histogram Editing .....	16
3.5 Boundary-Layer Velocity Histograms .....	17
3.6 Velocity Profiles from LDV Application .....	19
3.7 Particle Dynamics Downstream of a Normal Shock .....	19
3.8 Estimates of Uncertainty in Measured Velocity .....	21
4.0 CONCLUDING REMARKS .....	21
REFERENCES .....	23

## ILLUSTRATIONS

<u>Figure</u>	<u>Page</u>
1. Supersonic Wind Tunnel (A)	
a. Tunnel Assembly .....	25
b. Tunnel Test Section .....	25
c. Tunnel Stilling Chamber, Nozzle Section .....	26
2. Tunnel A Vertical Window Panels .....	27
3. Tunnel A Stilling Chamber Flow Velocity at Station of Seed Introduction .....	28
4. Model and Probe Systems Assembly .....	29
5. Probe Details	
a. Pitot Probe .....	30
b. Total Temperature Probe .....	30

<u>Figure</u>	<u>Page</u>
6. Schematic Diagram of Laser Doppler Velocimeter Optical System .....	31
7. Tunnel A Installation of LDV Traversing System .....	32
8. Atomizer Description	
a. Collison Nebulizer .....	33
b. Laskin Nozzle .....	33
9. Particle Size Distribution for Olive-Oil Droplets Produced by the Collison Nebulizer .....	34
10. Particle Size Distribution for Olive-Oil Droplets Produced by the Laskin Nozzle .....	35
11. Laminar Boundary-Layer Velocity Profiles Obtained Using Conventional Probes .....	36
12. Turbulent Boundary-Layer Velocity Profiles Obtained Using Conventional Probes .....	37
13. Transitional Boundary-Layer Velocity Profiles Obtained Using Conventional Probes .....	38
14. Concept of Particle Trajectories .....	39
15. Simultaneous Measurements in the Laminar Boundary Layer .....	40
16. Example of Histogram of Measured Velocity .....	41
17. Stacked Histograms for Laminar Boundary Layer	
a. Measured Histograms .....	42
b. Edited Histograms .....	42
18. Stacked Histograms for Turbulent Boundary Layer	
a. Measured Histograms .....	43
b. Edited Histograms .....	43
19. Stacked Histograms for Transitional Boundary Layer	
a. Measured Histograms .....	44
b. Edited Histograms .....	44
20. Laminar Boundary-Layer Velocity Profile Obtained Using LDV Techniques .....	45
21. Turbulent Boundary-Layer Velocity Profile Obtained Using LDV Techniques .....	46
22. Transitional Boundary-Layer Velocity Profile Obtained Using LDV Techniques .....	47
23. Law-of-the-Wall Velocity Profiles .....	48
24. Computed Particle Response to a Normal Shock Wave, $M = 4$	
a. $Re/ft = 0.6$ Million .....	49
b. $Re/ft = 3.0$ Million .....	49

<u>Figure</u>	<u>Page</u>
25. Measured Particle Response to a Normal Shock Wave, Particles from Collison Nebulizer, Back-Scattered Light	
a. $Re/ft = 0.65$ Million .....	50
b. $Re/ft = 3.1$ Million .....	50
26. Measured Particle Response to a Normal Shock Wave, Particles from Collison Nebulizer, Forward-Scattered Light	
a. $Re/ft = 0.65$ Million .....	51
b. $Re/ft = 3.1$ Million .....	51
27. Measured Particle Response to a Normal Shock Wave, Ambient Particles, $Re/ft = 3.1$ Million	
a. Back-Scattered Light .....	52
b. Forward-Scattered Light .....	52

### TABLE

1. Run Summary .....	53
NOMENCLATURE .....	54



## 1.0 INTRODUCTION

The purpose of this report is to document the results of an application of the nonintrusive Laser Doppler Velocimeter (LDV) technique to measure the boundary-layer velocity profiles on a sharp-cone model in the AEDC Supersonic Wind Tunnel (A) (Ref. 1). The history of applications of LDV techniques in Tunnel A can be briefly summarized. Measurements of free-stream flow velocity in the test section of Tunnel A, at Mach numbers from 1.5 to 5.5, were successfully made in 1982. The LDV techniques were then employed in 1983 in an attempt to measure mean-velocity profiles in a cone boundary layer at  $M = 4$ ; however, discrepancies existed between results inferred from the LDV data and those determined from pitot pressure surveys made at the same location on the model. In both the 1982 and the 1983 efforts, the free-stream flow was seeded using aluminum oxide (alumina) particles introduced in the tunnel stilling chamber. These particles had a nominal diameter of  $0.3\ \mu\text{m}$ , according to the manufacturer's specification. However, the evidence from the 1983 test indicates that the seed particles generally tended to agglomerate, and the resultant oversized particles were too large to execute the required change of velocity as the seed passed from the free stream into the model boundary layer. Particles of the same nominal size from the same manufacturer were used in an independent LDV measurements program at the AEDC at approximately the same time (Ref. 2). A mean particle diameter of  $1.7\ \mu\text{m}$  was inferred from these independent measurements and associated calculations discussed in Ref. 2, and the same diameter of  $1.7\ \mu\text{m}$  is believed to be applicable to the Tunnel A measurements in 1982 and 1983. Alternative seeding techniques were prepared for the present investigation to overcome the earlier problems. These techniques are discussed briefly in this report.

Laminar, transitional, and turbulent boundary-layer profiles were obtained on a sharp, 7-deg (half-angle) cone model at free-stream Mach number 4.0 with free-stream unit Reynolds numbers of 0.6, 1.0, and 3.0 million per foot at zero angle of attack. The Tunnel A flow was seeded, as required, using atomized olive-oil droplets introduced in the tunnel stilling chamber. A limited number of velocity measurements were acquired without seeding, relying on ambient particles in the tunnel flow.

Velocity profiles obtained using conventional (intrusive) pitot pressure and total temperature probe survey techniques and associated calculation procedures were selected at the outset as the basis for evaluating the adequacy of the LDV results and were acquired in conjunction with the LDV measurements, but not at the same time. The LDV results have been edited in many cases to remove what are believed to be spurious measurements from machine-generated noise or signals from large particles (Ref. 3).

## 2.0 APPARATUS

### 2.1 TEST FACILITY

Supersonic Wind Tunnel (A) (Fig. 1) is a continuous-flow, closed-circuit, variable density wind tunnel with an automatically driven flexible-plate-type nozzle and a 40- by 40-in. test section. The tunnel can be operated at Mach numbers from 1.5 to 6 at maximum stagnation pressures from 29 to 200 psia, respectively, and stagnation temperatures up to 750°R at Mach number 6. Minimum operating pressures range from about 1/10 to 1/20 of the maximum at each Mach number. The tunnel is equipped with a model injection system that allows removal of the model from the test section while the tunnel remains in operation. Optical access to the Tunnel A test section is furnished by schlieren-grade windows as illustrated in Fig. 2. With the test model located as indicated in Fig. 2, most of the aft 18 in. of the cone could be viewed through the two downstream vertical windows. However, the axial position of the model relative to the window panels can be adjusted using the model injection system. Seed particles added to the Tunnel A flow, when required for the laser measurements, were introduced into the tunnel stilling chamber at the port location shown in Fig. 1c. A description of the tunnel and airflow calibration information may be found in Ref. 4.

Stilling chamber centerline velocity for Tunnel A was determined from hot-wire anemometer measurements (1965) made at the port location where seed particles were introduced in the present investigation. These velocities are indicated in Fig. 3. The curve shown represents a fairing of the stilling chamber measurements that were made with the flexible-plate nozzle set for the indicated test-section Mach numbers. These data were acquired over a range of test conditions, including various stilling chamber pressure levels covering the available range, and with and without the addition of high-pressure air immediately upstream of the chamber to maintain the desired level of stagnation pressure. The spread in the measurements for each Mach number, indicated by the bars, is attributed to the wide range of conditions investigated.

### 2.2 TEST ARTICLE

The model was a 304 stainless-steel 7-deg (half-angle) cone with a basic sharp nose ( $RN = 0.0015$  in.), a virtual length of 40.0 in., and a base diameter of 9.82 in. Model instrumentation consisted of 24 surface pressure taps, 32 surface thermocouple gages, six hot-film constant-temperature surface anemometer gages, and six surface-mounted piezoelectric gages. Not all of these measurements were essential to the achievement of the primary test objective; certain measurements were included for evaluation or supplementary data. The locations of all of the surface taps and sensors are given in Ref. 1. The instruments

data. The locations of all of the surface taps and sensors are given in Ref. 1. The instruments used for these measurements and the associated precision index and bias of each instrument are listed in Ref. 1, also. Figure 2 indicates the upstream limit of the location of the model relative to the Tunnel A window panels. The Tunnel A model injection system permits the axial position of the model to be changed relative to the windows. This capability of adjusting model position was used in the present test to permit the LDV optics to be located in a more or less fixed, horizontal position relative to the windows.

In order to investigate the dynamics of the olive-oil droplets added to the tunnel flow for the LDV measurements, a special flow field with a large streamwise velocity gradient was needed. To provide such a flow field for the present investigation, the nose section of the cone model could be replaced with a right circular cylinder mounted with its axis in the vertical plane of the model and normal to the tunnel flow direction. The cylinder had a diameter of 2.0 in. and an axial length of 12.0 in. For free-stream Mach number 4.0, the normal shock wave generated by the cylinder had a standoff distance of approximately 0.54 in. in the vertical plane of the model. The simplicity of the model change made it feasible to investigate particle dynamics whenever seeding procedures were altered. The model was positioned in the tunnel test section so that the flow field between the shock wave and the generating cylinder could be viewed through the downstream vertical window panel used for all of the LDV measurements. The LDV instrument was used to measure the local velocity of the seed particles at closely spaced intervals from immediately upstream of the normal shock wave to the surface of the cylinder. The measured velocity of the olive-oil droplets, decelerated upon passing through the shock, was compared to theory as discussed by Nichols in Ref. 5. Comparison of the measured velocities with theoretical velocities for olive-oil droplets of each of several diameters provided a means for estimating the effective size of the droplets produced by the various seeding procedures employed, for any given free-stream unit Reynolds number.

### **2.3 BOUNDARY-LAYER SURVEY MECHANISM**

Boundary-layer surveys were made using a sting-mounted probing mechanism (Fig. 4). The longitudinal axis of the probe drive mechanism was inclined 7-deg with respect to the model axis. The surveys across the boundary layer were made in the direction normal to the model surface. The model centerline was located 2 in. below tunnel centerline so that the presence of the probe drive mechanism would not interfere with the tunnel wall boundary layer. In the present test, all boundary-layer surveys with the probe mechanism were made at  $XSTA = 35.5$  in.

## 2.4 BOUNDARY-LAYER SURVEY PROBES

The conventional probes used to survey the model boundary layer were mounted in a holder (Fig. 4) attached to the survey mechanism. The pitot pressure probe (Fig. 5) had a cylindrical tip of 0.006-in. ID. This probe was fabricated by cold-drawing a stainless-steel tube through a set of wire-drawing dies until the desired inside diameter was obtained. The outside surface of the drawn tube was subsequently electropolished to a diameter of 0.012 in.

The unshielded total temperature probe (Fig. 5) was fabricated from a length of sheathed thermocouple wire (0.020-in. OD) with two 0.004-in.-diam wires. The wires were bared for a length of approximately 0.015 in., and a Chromel® -Alumel® thermocouple junction of approximately 0.005-in. diam was made.

## 2.5 LASER DOPPLER VELOCIMETER MEASUREMENT SYSTEM

An optical schematic of the LDV system used for the present test measurements is shown in Fig. 6. The system was oriented to measure two orthogonal velocity components in the vertical plane of the model, along axes designated  $x'$  and  $z'$  (See the insert in Fig. 6), which were respectively parallel and normal to the surface of the 7-deg cone model.

The two LDV measurement axes were implemented using the two most powerful spectral lines produced by an argon ion laser, (1) the 514.5-nm (green) line, at approximately 1.4 w, along the  $x'$  axis and (2) the 488.0-nm (blue) line, at approximately 1.3 w, along the  $z'$  axis. The transmitting optics system is designated as a moving-fringe, dual-beam system. The LDV measurement volume for the green beam was an ellipsoid of revolution (prolate spheroid) with a 1.5-mm major-axis length and a 0.4-mm minor-axes length. The blue beam had a corresponding volume with a major axis of 2.0-mm length and minor axes of 0.8-mm length. Two different scattered-light receiver systems were employed, a back-scatter system and a forward-scatter system. The former system accommodated measurements in both the  $x'$  and  $z'$  directions, whereas the latter system accommodated measurements in the  $x'$  direction only. The forward-scatter receiver represented an alternative technique not used in the 1982 and 1983 efforts (See Section 1.0). This technique was included in the present investigation because the forward-scatter light levels are usually 10 to 50 times greater than those produced by back-scattered light. This signal-level advantage would permit velocity measurements to be derived from smaller particles in the flow than those required for back-scattered light. Considerations of particle dynamics indicate that particle size must be as small as practical (0.5  $\mu\text{m}$  or less).

The LDV data from the scattered-light receivers were handled in a conventional manner by an AEDC-developed counter-type processor. This counter processor measures the period of the scattered-light signal when a particle intercepts the LDV measurement-volume fringes. The inverse of the signal period is traditionally referred to as the "Doppler" frequency. The LDV data acquisition system performs the inversion of the signal period to obtain the Doppler frequency and then multiplies by the fringe spacing to determine a discrete velocity sample. The data acquisition system was programmed to handle 1,000 velocity samples per component per data point. Additional details of the counter processor are given in Refs. 6 and 7. The computer-controlled data acquisition system is described in Ref. 6.

In addition to the conventional handling of the LDV data discussed in the preceding paragraph, an AEDC-developed discrete Fourier transform (DFT) processor was available for use with any two of the three signals acquired (two back scatter, one forward scatter) during the measurements. The DFT was developed to address the problem of the LDV technique of acquiring velocity measurements of acceptable quality from particles in the submicron-size range. In the present application, the DFT processor was operated in the optional configuration as a single-channel instrument and generally was applied to the forward-scatter signals. The principal components of this processor are a high-speed waveform recorder and a Fourier transform computer. The waveform from the system photodetector is recorded by the waveform recorder, which functions as a high-speed analog-to-digital converter. The digitized waveform data are then Fourier transformed by the computer to obtain a measure of the Doppler frequency. Details of the DFT processor are discussed in Ref. 8.

## 2.6 LASER DOPPLER VELOCIMETER TRAVERSING SYSTEM

The LDV laser, transmitting optics, and back-scattered light receiver were mounted on a common optics table that, in turn, was mounted on a three-axis traversing system (Fig. 7). The axes of traverse were aligned with the x, y, and z tunnel coordinate axes prior to the beginning of the test program. The traverse motion on each axis was programmed in integral multiples of 0.001 in. using the associated control systems of the drive mechanism. The nominal ranges of travel in the three directions were x:20 in., y:16 in., and z:11 in. In the present testing, the LDV measurement volume was traversed across the boundary layer in the vertical direction using the z drive. The position along the model selected for surveys was set using the x drive.

The present LDV investigation furnished the first opportunity to evaluate a forward-scattered light receiver in Tunnel A. This application used a proof-of-principle scheme involving available equipment and somewhat inefficient and time-consuming manual operations. To acquire boundary-layer profile data, the transmitting optics system usually was traversed

vertically, and an attempt was made to follow this motion precisely with an independent traverse of the forward-scatter receiver. To accomplish the coordinated movement of two optical systems separated by the wind tunnel, the transmitter traverse motion was sensed using a semiconductor position sensor mounted on the receiver traverse mechanism and oriented to intercept a laser beam from a small He-Ne laser mounted on the transmitter optics table. The traversing of the receiver was controlled manually to null the position sensor each time the transmitter was moved. While procedures for this operation were being established, it was found that the exterior walls of the pressure tank that houses the Tunnel A model injection system were subject to small but significant deflections when the tank was depressurized prior to model injection. Inasmuch as the forward-scatter-receiver traverse mechanism had been mounted on the top of the injection tank, the critical optical alignment of the receiver with the transmitter had to be done with the tank depressurized. An alternative procedure was used for some of the surveys; the LDV transmitting optics and the forward-scatter light receiver were aligned and then held in position relative to the tunnel while the model was traversed axially in the tunnel using the model injection system (Section 2.2). The precision of the model traverse is generally lower than that of the optics traverse system; but optical alignment was easier to maintain if the model was moved instead of the optics. For present purposes, surveys made holding the optics stationary were assumed to be essentially equivalent to those made holding the model stationary. The nominal axial station of the model was  $XSTA = 35$  in. for all boundary-layer surveys for LDV measurements. Surveys of the special flow field used to investigate the dynamics of seed particles in the flow (Section 2.2) were made by moving the model while the optics traverse system was held stationary.

## 2.7 TUNNEL FLOW SEEDING TECHNIQUES

Laser velocimeter systems rely upon light scattered from particles in the flow to make it possible to infer the velocity of the flow. These systems cannot detect molecular-size particles but are constrained by the light-scattering considerations to particles with diameters of the order of  $0.5\text{ }\mu\text{m}$  or larger. In a given tunnel, the ambient particle content of the flow may be sufficient for measurements; however, investigations generally have found seeding of flow fields is required in order to achieve a productive data rate.

Exploratory measurements made in the free stream of the Tunnel A test section in 1979 (Ref. 9) using a laser transit anemometer instrument indicated that the flow (at Mach 4.5) contained very few particles of appropriate size for laser-based measurements. Nevertheless, over a period of 5 sec a sufficient number of particles was detected at that time to allow a qualified inference of free-stream velocity that was within 0.6 percent of the stated tunnel velocity for the given test conditions. The ambient free-stream particles were estimated to be between  $0.2\text{-}$  and  $0.4\text{-}\mu\text{m}$  diam, as reported in Ref. 9.

The ambient particle content of the flow was investigated again in the present effort. First, the laminar boundary layer on the cone model was examined using the LDV instrument, and it was determined that the number of ambient particles in the tunnel flow was not sufficient to provide an acceptable data rate for the desired LDV measurements. Based on this information, it was considered necessary to seed the flow artificially. Second, measurements made to examine the dynamics of the ambient particles in the tunnel, discussed in Section 3.7 of the present report, indicate that these particles were larger than  $0.5\text{ }\mu\text{m}$  in diam and that some particles of  $1.0\text{-}\mu\text{m}$  diam were present. It is important to note that differences in the data rates that can be achieved at different times using the ambient particles are strongly dependent on the recent history of the tunnel circuit. For example, any modification of the circuit or any plant procedure that causes a spill of desiccant from the drier beds of the circuit could affect particle content of the "unseeded" flow.

In recent years, prior to the present investigation, only solid-particle aerosol generators had been used at the AEDC to introduce particles into the aerodynamic and aeropropulsion test facility flows for laser velocimetry applications. However, the application of the fringe-type velocimeter (LDV) to supersonic boundary-layer velocity measurements in 1983 demonstrated that control of the particle size distribution from such generators is not a simple task, principally because of the tendency of the small, solid particles to agglomerate. A more promising approach, at least for the stilling chamber temperatures associated with Tunnel A, appeared to be the use of liquid atomization techniques to produce seed particles. On this basis, two different atomization techniques were employed in the present investigation, a commercially available Collison nebulizer (TSI Model 9306 Atomizer) and a Laskin nozzle fabricated by the AEDC. Olive oil was chosen as the liquid to be atomized, principally because it is not toxic and has been used successfully by other investigators; for example, see Ref. 10. The particle size characteristics of both of the atomizers used in the testing were investigated for olive oil. The techniques used to determine the size distributions are outlined in Ref. 11, and the results are summarized in the following paragraphs.

The principle of the Collison nebulizer (Ref. 12) is illustrated in Fig. 8a. A jet of gas (air, in the present case) is used to shear a column of flowing liquid (olive oil, in the present case) to create an aerosol made up of a large number of small, liquid droplets. The larger droplets are generally eliminated by impact upon a solid surface located downstream of the gas jet. The droplets produced by the nebulizer used in the present effort had a size distribution with 90 percent of the droplets in the size range from approximately  $0.1$  to  $0.45\text{ }\mu\text{m}$  and about 10 percent in the range from  $0.45$  to  $2.0\text{ }\mu\text{m}$  (Fig. 9).

The Laskin nozzle was of the same design as discussed in Ref. 10, and the principle of the nozzle is illustrated in Fig. 8b. An aspirated liquid column is sheared using an air jet,

and a liquid droplet aerosol is produced. In the present case, the olive-oil droplets produced by the Laskin nozzle had a size distribution (Fig. 10) similar to the droplets produced by the nebulizer, but with 90 percent of the droplets occurring in the size range from 0.1 to 0.6  $\mu\text{m}$ , a wider range than for the nebulizer.

The olive-oil droplets were introduced into the Tunnel A flow using a port in the tunnel stilling chamber (Fig. 1c). A stainless-steel tube of 1.0-in. diam guided the droplets from the generator to the centerline of the stilling chamber, where the seed particles were released in the direction of the tunnel flow. The two atomizers had a common size of tube fitting to facilitate interchange of the generators.

### 3.0 RESULTS AND DISCUSSION

Surveys were made to obtain velocity profiles of the boundary layer on the sharp cone model at stations near the model base to evaluate the capability of the laser Doppler velocimeter instrument for nonintrusive velocity measurements in supersonic flow, using current capability for seeding the flow. The basis for the evaluation was a set of velocity profiles obtained using conventional probing techniques. Differences in the survey stations and in the traverse directions of the nonintrusive and conventional surveys (See Sections 2.3 and 2.6) were small and have been taken into account by appropriately normalizing the parameters.

#### 3.1 CONVENTIONAL TECHNIQUES

Plots of boundary-layer velocity profiles determined from the pitot pressure and total temperature measurements have been presented in normalized form. Velocities have been normalized using boundary-layer edge velocity, which was determined for each profile from measurements made at heights greater than  $1.2 \delta$ . The distance from the model surface to each station in the profile has been nondimensionalized using the total boundary-layer thickness, which was defined as the height corresponding to  $u/u_e = 0.995$  and which was determined by interpolation among the profile data points. Redundant profile measurements were made to confirm the results from the conventional probing technique.

The data for the conventional probe results for the laminar boundary layer are presented in Fig. 11. Points measured in the lower 35 percent of the layer exhibited evidence of interference with the flow caused by the presence of the probes. The theory shown with the data is the laminar profile generated using the computer code discussed in Refs. 13 and 14 for the nominal test conditions. The value of  $\delta$  is defined in the code as the height for which  $u/u_e = 0.995$ . The agreement between data and theory is seen to be good.



The velocity profiles for the case of the turbulent boundary layer, as determined from the conventional probe surveys, are shown in Fig. 12. Interference with the boundary-layer flow caused by the presence of the probes was not an apparent problem in these profiles. The data are shown with the simple  $1/7$ -power relation often used to describe the turbulent-layer profile (Ref. 15, p. 637, for example). This relation is considered adequate for the present evaluation.

A velocity profile for the case of a transitional boundary layer at the survey station is presented in Fig. 13. Probe interference does not appear to be a problem in this profile. Theoretical curves for both laminar and turbulent profiles are shown for reference.

### 3.2 SEEDING OF THE FLOW

The seeding of the tunnel flow from the stilling chamber established a core of seeded flow in the Tunnel A test section that was estimated to extend 6 to 8 in. on either side of the tunnel centerline in the lateral and vertical directions. The extent of this seeded region was altered by the conical flow field generated by the sharp-cone model. Ideally, the seed would change direction instantaneously upon encountering the conical shock wave and assume the local flow velocity parallel to the model surface. Of course, the presence of the boundary layer on the model would impose further changes of velocity upon a given particle depending on the depth of its penetration into the layer.

In reality, the particles require a finite length of time to adjust to a change of flow-field velocity and in that recovery period will have traveled some finite distance characterized by a velocity lag. This recovery distance, according to Donald Barnett (private communication, June 1982), can exceed the scale of the flow phenomenon, that is, the thickness of the boundary layer or the width of the shock wave (Ref. 5), even for particles of  $1\text{-}\mu\text{m}$  nominal size. Reduction of particle size to alleviate the velocity lag problem has severe limitations because the particles must scatter sufficient light for detection in order to serve their intended purpose. In the present investigation, particle detection was attempted with each of three techniques (See Section 2.5), (1) back-scattered light signals processed by a counter processor, (2) forward-scattered light signals processed by a counter processor, and (3) forward-scattered light signals processed by a discrete Fourier transform processor.

A conceptual sketch of the varied histories of particles intercepted by the LDV measurement volume is suggested in Fig. 14 for the case of a laminar boundary layer. The concept includes particles that have become reconciled to local boundary-layer velocity, those that have only recently entered the layer and are still traveling with essentially free-stream velocity, and particles of essentially all intermediate velocities. Still other particles may have impacted on

the model surface and rebounded so that they enter the probe volume obliquely from below; these have been included in the sketch, also.

### 3.3 SIMULTANEOUS COMPONENT MEASUREMENTS

The substantiation of the concept shown in Fig. 14, or its equivalent, was found among simultaneous LDV measurements in the directions parallel and normal to the model surface. These data were acquired by programming the data acquisition system to count only those particles whose passage is sensed simultaneously by the parallel (green) beam and the normal (blue) beam. The coincident measurement of both velocity components provides the means to determine the particle-velocity vector.

A typical example of the information that was obtained by using the simultaneous-measurements mode during surveys of the laminar boundary layer is shown in Fig. 15. Note that these data, which were acquired 0.020 in. above the model surface, have been rotated into the x-z axes system. Each of the 1,000 points in Fig. 15 represents the tip of a vector from the origin of the axes. A vector representing the mean velocity has an angle of approximately 7 deg with respect to the abscissa axis; but it is obvious from the figure that a wide range of velocities was found among the particles passing through the two measurement volumes simultaneously. It is seen in the scatter of points that many particles were traveling at very high velocity, and some particles were traveling away from the model. The associated histograms for the x and z axes are also included in Fig. 15. The width of each histogram "bin" represents a velocity range of 20 ft/sec.

For most of the data acquired in the testing, coincident measurements were not required; that is, the velocity components were sensed independently so that velocity histograms were independent, and velocity vector angles could not be determined. In succeeding presentations in this report, only the velocity in the direction parallel to the model surface is discussed, because the average value of the normal component was essentially zero for each set of measurements.

### 3.4 HISTOGRAM EDITING

A histogram of measured velocities for one data set is shown in Fig. 16 to emphasize how the presence of particles traveling through the measurement volume with velocities greater than the local velocity can complicate the velocimeter results. The mean and standard deviation of the set of all measured velocities was calculated and a normal probability density curve was constructed from this minimum information, the curve marked "unedited data" in the figure. Theoretical calculations and independent measurements using conventional techniques

indicated that the prominent peak toward the low-velocity end of the histogram represented the particles properly following the flow. The remainder of the histogram was assumed to represent particles that were too large for complete relaxation of their velocities within the distance available. Also, the velocity histograms in general may contain a low background of spurious noise. This is likely in the present results where the effort was made to obtain data from the smallest particles possible because of the expected particle dynamics problems in the low-density/high-velocity flow. For this purpose, the system sensitivity was set on the very edge of the noise level with a good probability that some noise would be processed. However, the noise is random in nature and the effects, especially on mean-velocity determination, can be removed from the final results by a data reduction/editing scheme. The general editing applied in the present investigation was simply to discard any velocity bin that did not contain at least 10 measurements. After the histogram of Fig. 16 had been edited to eliminate the velocities of relatively low probability and the noise effects, the remaining velocities were used to calculate a new mean and standard deviation, and the new normal probability density curve shown. In the data presentation to follow, many of the histograms represent data edited in the manner just described; however, in some cases it was not obvious where editing was justified. It is strongly recommended that the data acquisition in future LDV applications also be done without any concurrent editing. The flexibility retained by posttest editing of the unadulterated response of the LDV instrument is needed with the present state of the art.

### 3.5 BOUNDARY-LAYER VELOCITY HISTOGRAMS

A collection of histograms obtained from a survey of a laminar boundary layer is shown in Fig. 17. Each histogram in Fig. 17a represents measurements at one position in the boundary layer, and the histograms have been stacked in a pattern to indicate (by position of the baselines) the relative locations of the measurement stations with respect to the model surface. These histograms of raw, unedited data show the low, random background of spurious noise and, in some regions, the particle dynamics effects previously shown in Fig. 16. Care must be taken in using the mean value of the observed velocities at any station. It is also important to recognize that the use of the standard deviation of the measured velocities as an indication of velocity fluctuation ("turbulence") is not correct, at least until all extraneous velocity samples have been rejected. The stacked, edited histograms for the laminar boundary-layer velocity profile are shown in Fig. 17b. Calculations of a theoretical particle-velocity distribution were made by Nichols (Ref. 5) for the measured conditions that pertain to Fig. 17 for each of several diameters of olive-oil droplets. These calculated particle-velocity profiles are included in Fig. 17b for comparison with the edited LDV data. The calculations indicate that an olive-oil droplet diameter of  $0.5 \mu\text{m}$  would be sufficiently small to yield adequate mean-flow LDV velocity profiles in the laminar boundary layer of the present investigation. It should be noted

that measurements shown in the histograms in Fig. 17b indicate that the LDV instrument was indeed capable of detecting droplets of  $0.5\text{-}\mu\text{m}$  diam. However, the measurement histograms seem to indicate that the diameter of the majority of the droplets detected was larger than  $0.5\text{ }\mu\text{m}$ . By contrast, the seed size distribution in Fig. 9 indicates that the majority of the droplets produced by the Collison nebulizer was smaller than  $0.5\text{ }\mu\text{m}$  in diam. The apparent discrepancy can be explained by considering the distribution of light intensity in the LDV measurement volume. The measurement volume has a Gaussian intensity distribution with the most intense fringes concentrated near the center of the volume (Ref. 7). Inasmuch as the light scattered by particles decreases almost exponentially with particle size, small particles would have to travel through the center of the measurement volume to cross the required eight fringes and scatter sufficient light to be detected. On the other hand, large particles could probably produce a detectable signal by traveling through any part of the measurement volume containing at least eight fringes. As a result, the "effective measurement volume" is a function of particle size, and the smaller particles have a lower probability of being detected by the LDV processor. These findings indicate that, at least with the present LDV system, it was virtually impossible to "overwhelm" a small, but significant, number of large particles by means of a much greater number of small particles.

Stacked histograms of measurements of particle velocities across a turbulent boundary layer are presented in Fig. 18a. Based upon the response of flush-mounted hot-film anemometer gages, the region of boundary-layer transition to turbulence began ahead of  $XSTA = 12$  in. and was completed by  $XSTA = 24$  in. for the selected test condition. The measurement histograms at all positions in the boundary layer contain the velocities of numerous extraneous particles. An effort was made to edit the velocity distributions. Justification for the editing was discussed briefly in Ref. 3 using, in part, data from the present investigation. The stacked, edited histograms for the turbulent boundary layer are presented in Fig. 18b. Near the edge of the layer, the editing technique produced a relatively narrow distribution of velocities; whereas in the lower one-third of the layer, the histograms were spread over a wide range of velocities.

In Fig. 19a, stacked measurement histograms for a transitional boundary layer are shown. The hot-film gages indicated that the region of transition began at  $XSTA = 30$  in. and extended beyond the model base for  $Re/ft = 1.0$  million. Except near the outer edge of the layer, where the histograms resembled those found in the laminar case, the character of the histograms for this "state" of transition was distinct from either the laminar or the turbulent cases. Results of the editing of the measurements are shown in the stacked histograms in Fig. 19b.

### 3.6 VELOCITY PROFILES FROM LDV APPLICATION

In Fig. 20, velocity profiles determined from LDV-edited results for the case of the laminar boundary layer are shown with a theoretical profile for comparison. The plot parameters have been normalized in the same way as those in Figs. 11, 12, and 13 as discussed earlier. The theory shown with the data in Fig. 20 is the laminar profile shown in Fig. 11, which was generated using the computer code discussed in Refs. 13 and 14. It is seen that the maximum lag of particle velocity occurred near the middle of the layer rather than near the model surface. It is also apparent from these results that the LDV can be very useful for velocity measurements close to the model surface where conventional probes interfere with the local flow. The relative size of the LDV measurement volume, slightly more than 10 percent of the total thickness of the laminar boundary layer for the test conditions and model station of the present survey, is indicated in Fig. 20. It should be noted that the probe height is zero when the center of the measurement volume is located at the model surface by the convention usually adopted. However, in this position, one-half of the measurement volume is subject to the passage of particles resulting in a nonzero velocity indication. Moreover, any time a portion of the measurement volume is in contact with the surface, a positive velocity bias exists (See Ref. 16) in the results, as shown in Fig. 20 for the lower 10 percent of the layer.

Velocity profiles obtained using LDV measurements in a turbulent layer are shown in Fig. 21. The data are shown with the  $1/7$ -power relation for comparison. The LDV measurements from a transitional boundary layer were the source of the velocity profile presented in Fig. 22. As in the case of Fig. 13, theoretical curves for both laminar and turbulent profiles are shown for reference.

Three of the boundary-layer velocity profiles obtained using the LDV techniques and included in Figs. 20, 21, and 22 are presented in Fig. 23 in the format used for "law-of-the-wall" velocity profile correlation, which has been found useful as a means of relating the profiles to skin friction. The value of the effective shear velocity used in normalizing the measurements to obtain the law-of-the-wall parameters is indicated for each profile. The expression shown for the fairing of the LDV data for the turbulent case contains the usual value of 2.5 for the multiplying coefficient (which is the reciprocal of the von Kármán constant, 0.4), whereas the value of 4.3 for the intercept was chosen to yield a good fairing among the present LDV data. Similar findings were reported in the law-of-the-wall analysis of Ref. 17.

### 3.7 PARTICLE DYNAMICS DOWNSTREAM OF A NORMAL SHOCK

The normal cylinder configuration (Section 2.2) was used to generate an extreme velocity gradient in the seeded test-section flow. Surveys were made of the resultant flow field using the LDV to observe the velocity relaxation of the seed particles. Horizontal surveys from just upstream of the detached normal shock wave to the surface of the cylinder were made

holding the LDV measurement volume in fixed position relative to the tunnel and using the Tunnel A model injection system (Section 2.1) to reposition the cylinder relative to the measurement volume.

Before consideration is given to measurements made with the cylinder bow shock wave, it is appropriate to consider the theoretical response of olive-oil droplets to the flow field. Computed responses for droplets of various diameters are shown in Fig. 24 for two conditions at Mach 4, free-stream unit Reynolds numbers of 0.6 and 3.0 million per ft. These calculations were made by Nichols and were presented, in part, in Ref. 5. Upstream of the bow shock, there would be sufficient distance from the point of seed introduction (Section 2.6) for all particles to attain free-stream velocity. The calculations indicate, however, that once the droplets pass through the bow shock, the velocity recovery distance is a function of droplet size and flow-field conditions. At sufficient distance downstream of the shock, the droplets will relax to the air velocity, and a low-velocity mode will form in the histogram. This mode will be initiated by the smallest droplets and will grow as successive droplets relax to the local velocity. For any given droplet size, the distance required for velocity relaxation decreases when unit Reynolds number is increased. For the test condition that yielded a laminar boundary layer on the cone model during the present investigation, the calculations (Fig. 24a) indicate that olive-oil droplets of  $0.5\text{-}\mu\text{m}$  diam will exhibit significant velocity lag in a flow with a severe velocity gradient (See the discussion of Fig. 17b in Section 3.5.).

Selected results obtained from surveys of the flow field of the cylinder/shock wave configuration are shown in Figs. 25, 26, and 27. Histograms for each survey have been stacked according to location with respect to the bow shock. In each figure, the theoretical fluid velocity is shown for comparison with the recovery velocity exhibited by particles of finite size actually in the flow. The results shown in Figs. 25 and 26 were obtained with the Collison nebulizer that was used for the boundary-layer profile data discussed earlier in this report. In Fig. 25, data acquired using back-scattered light are shown for two free-stream unit Reynolds numbers. The results indicate that the distance required for velocity recovery was reduced by the increase of unit Reynolds number, in agreement with the trend shown for theory in Fig. 24. The measurements also indicate that the flow seeded using the nebulizer contained droplets with a wide size distribution. Data acquired at the same time, but using forward-scattered light, are presented in Fig. 26. In the latter case, the distance required for velocity recovery was shorter for a given unit Reynolds number, indicating, as expected (Section 2.5), that the forward-scatter technique was able to detect smaller droplets. Results obtained using the Laskin nozzle (Section 2.7) to seed the flow were very similar to those associated with the Collison nebulizer, but indicate the Laskin nozzle produced some slightly smaller droplets as well as fewer large droplets. The results are presented by Heltsley in Fig. 21 of Ref. 3; indeed, data from the present investigation served as the basis for much of the discussion in Refs. 3 and 5.

The unseeded flow in the Tunnel A test section for a unit Reynolds number of 3 million per ft was also investigated, and results are presented in Fig. 27 for both back-scatter and forward-scatter signals. For the case of back-scattered light (Fig. 27a), there is no histogram shown for the free stream because the number of ambient particles large enough to be detected was insufficient. Downstream of the shock wave, some of the ambient particles were detected with back-scattered light, but their population was very small. The ambient particles were more readily detected in the case of forward-scattered light (Fig. 27b), but the associated data rate was low. In both cases, the ambient particles that were detected exhibited very short relaxation distances, indicative of their small size.

### 3.8 ESTIMATES OF UNCERTAINTY IN MEASURED VELOCITY

Estimates have been made of the uncertainty of the local velocity that was calculated from the pressures measured by the pitot probe and model surface orifice and total temperature measured by the survey probe, based on measurement uncertainties for the various instruments used. These estimates were made near the midheight of the boundary layer for both the laminar and turbulent cases and have been listed below. The simple difference between velocity obtained using the LDV and velocity calculated from the theory was determined at approximately the same location in the profiles. These differences are also listed in the following table for both measured (unedited) and edited LDV results. The positive differences indicate the LDV velocity was higher than theory.

**Velocity Uncertainties and Differences (At  $z' = 0.5 \delta$ )**

<u>Technique</u>	<u>Laminar Case, percent</u>	<u>Turbulent Case, percent</u>
Conventional Probes	$\pm 4.5$	$\pm 1.0$
LDV (Measured)	+ 9.1	+ 1.0
LDV (Edited)	+ 4.5	+ 1.0

NOTE: All percentages are with respect to local velocity.

### 4.0 CONCLUDING REMARKS

A two-component laser Doppler velocimeter was used for the measurement of mean-velocity profiles across the boundary layer on a 7-deg (half-angle) sharp-cone model in the AEDC Supersonic Wind Tunnel (A). With a free-stream Mach number of 4 and free-stream unit Reynolds numbers of 0.66, 1.0, and 3.0 million per ft, the profiles at the survey station were laminar, transitional, and turbulent, respectively. The LDV measurements were made

in each of these three layers. Velocity profiles were also obtained from pitot pressure and total temperature measurements made at an adjacent model station. The tunnel flow was seeded with olive-oil droplets after it was determined that the ambient particles in the flow generally did not provide an acceptable data rate for the LDV measurements. The seed particles were introduced into the flow in the tunnel stilling chamber.

The results obtained by this investigation demonstrate the following:

1. The mean-velocity profiles can be measured across the boundary layer of a model in supersonic flow using LDV techniques within acceptable limits of uncertainty provided (a) seed particles of appropriate size are found in the tunnel flow or can be added to the flow, and (b) a systematic editing procedure is available when the results are evaluated to eliminate velocities of relatively low probability and effects of a background of spurious noise.
2. The maximum lag of particle velocity in the laminar boundary layer occurred near the middle of the layer rather than near the model surface.
3. The LDV technique can be especially useful for velocity measurements close to the model surface where conventional probes interfere with the local flow, but a measurement bias must be taken into account when the LDV measurement volume intersects with the surface.
4. The LDV technique that uses forward-scattered light to observe the passage of particles offers a significant advantage over the technique that uses back-scattered light, because the former can detect significantly smaller particles with a consequent improvement in the handling of measurement difficulties related to particle dynamics. Application of the forward-scatter technique requires special attention in coordinating the transmitter traverse motion and the receiver traverse motion in order to maintain alignment. Care is also required in mounting both traverses, so that the alignment is not disturbed by the movement of tunnel surfaces caused by routine tunnel operations.
5. The application of the LDV technique is enhanced by having access to a flow field containing a significant velocity gradient in which evaluation of particle dynamics can be made.

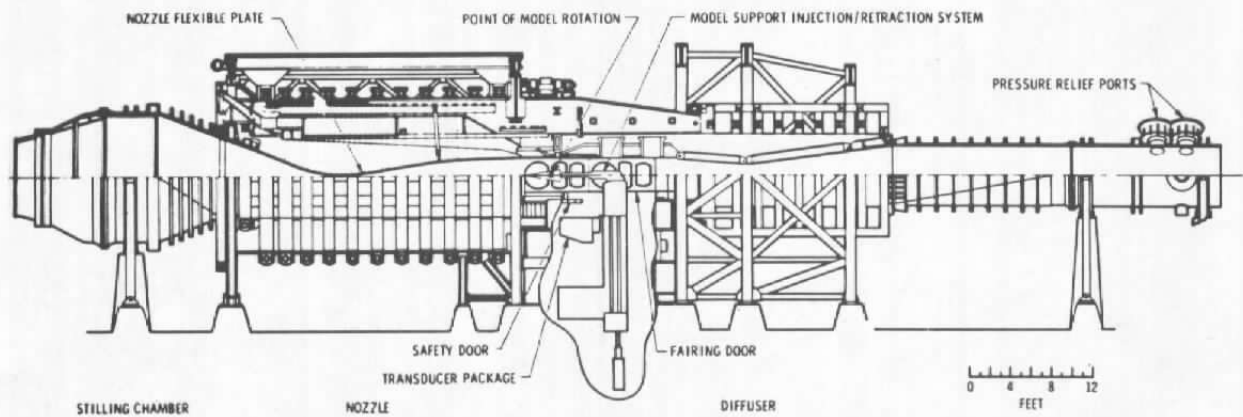


6. The naturally occurring particles observed during the present study in Tunnel A exhibited good recovery of velocity but were not numerous enough to produce an acceptable data rate.

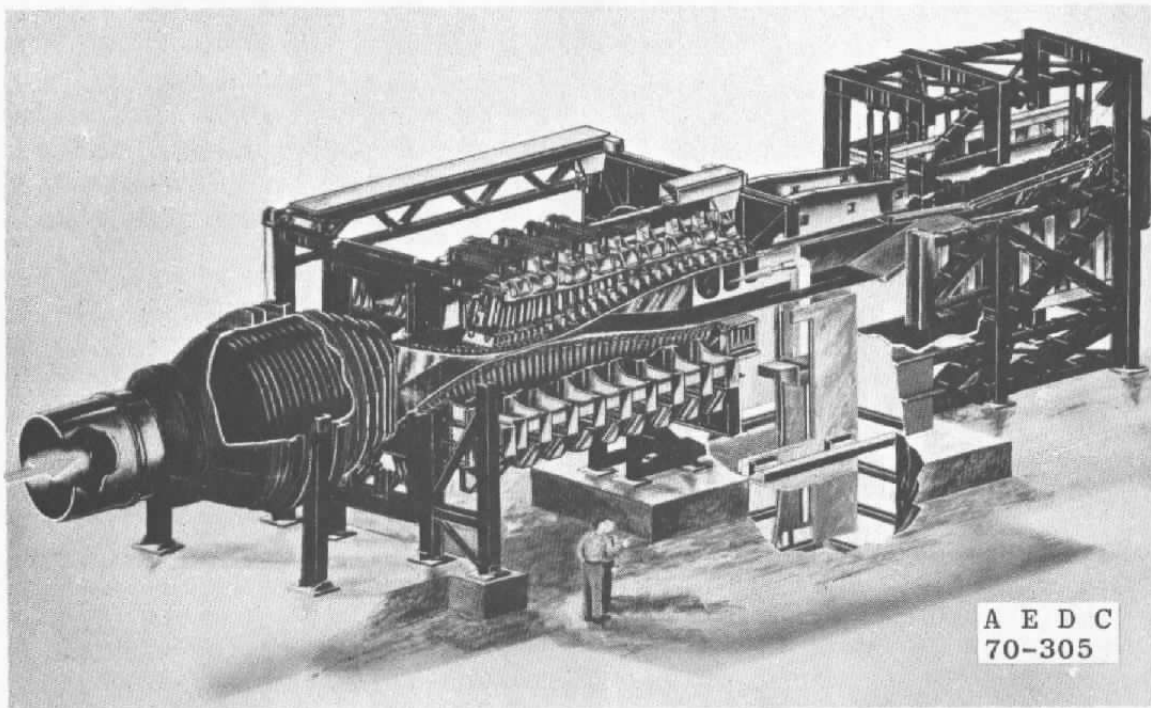
## REFERENCES

1. Marquart, E. J., Donaldson, J. C., and Simons, S. A. "Laser Doppler Velocimeter (LDV) and Pitot Probe Measurements on a 7-Deg Cone at Mach 4." AEDC-TSR-84-V32, October 1984.
2. Heltsley, Fred L., Walker, Billy J., and Nichols, Robert H. "Transonic Nozzle-Afterbody Flow Field Measurements Using a Laser Doppler Velocimeter." Presented at the 53rd Meeting of Fluid Dynamics Panel Symposium on Wind Tunnels and Testing Techniques, Cesme, Turkey, September 26-29, 1983.
3. Heltsley, Fred L. "Recent Experience in Seeding Transonic/Supersonic Flows at AEDC." Proceedings of Wind Tunnel Seeding Systems for Laser Velocimeters. A workshop held at NASA Langley Research Center, Hampton, Virginia, March 19-20, 1985. NASA CP-2393, pp. 121-140.
4. Boudreau, A. H. "Performance and Operational Characteristics of AEDC/VKF Tunnels A, B, and C." AEDC-TR-80-48 (AD-A102614), July 1981.
5. Nichols, Robert H. "The Effect of Particle Dynamics on Turbulence Measurements with the Laser Doppler Velocimeter." Dissertation, University of Tennessee, Knoxville, Tennessee, June 1986.
6. Crosswy, F. L., Heltsley, F. L., and Sherrouse, P. M. "Recent Development and Applications of a Three-Component Laser Doppler Velocimeter." Proceedings of the ISA 28th International Instrumentation Symposium Part 2, Las Vegas, Nevada, May 3-6, 1982, pp. 679-705.
7. Kalb, H. T., Brayton, D. B., and McClure, J. A. "Laser Velocimetry Data Processing." AEDC-TR-73-116 (AD-766418), September 1973.
8. Kalb, H. T. and Crosswy, F. L. "Discrete Fourier Transform Signal Processor for Laser Doppler Velocimetry." AEDC-TR-83-46 (AD-B078684L), December 1983.

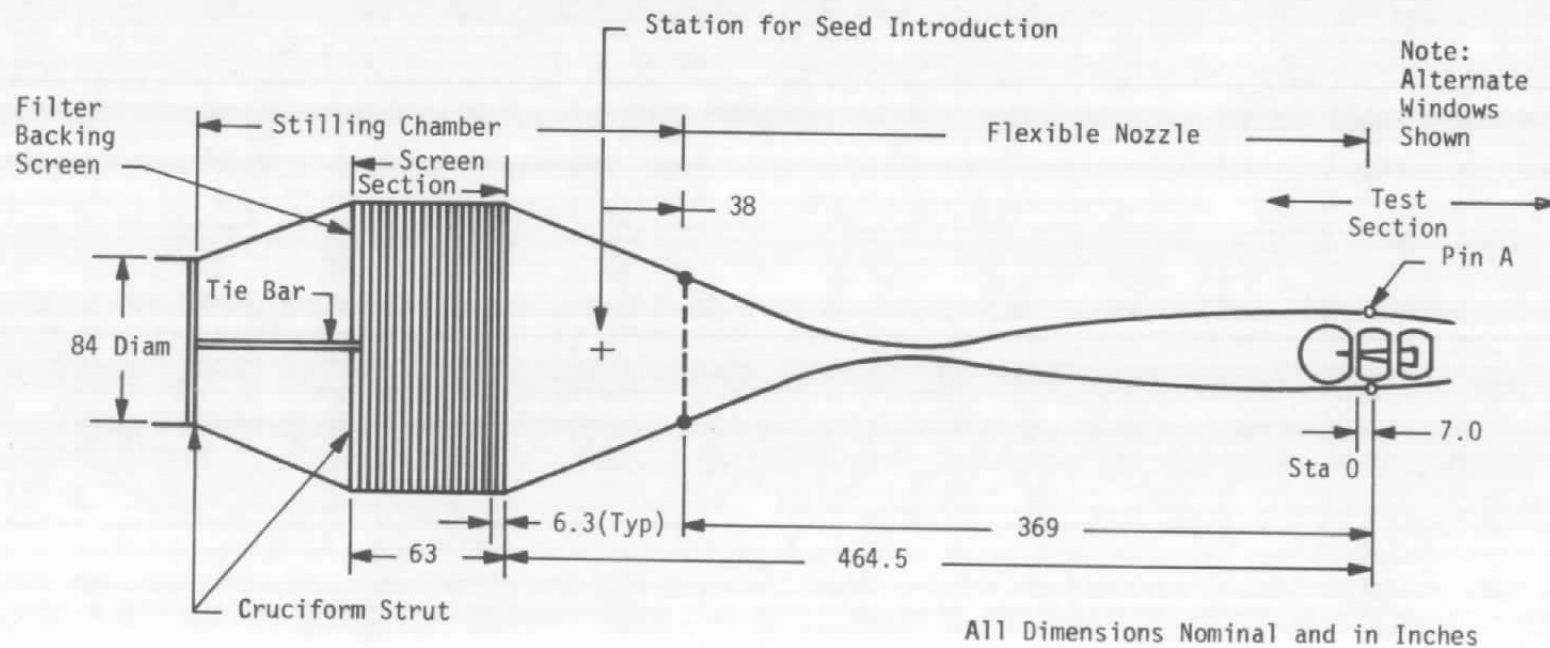
9. Smart, A. E. and Mayo, W. T., Jr. "Experimental and Analytical Development of the Application of a Transit Laser Velocimeter." AEDC-TR-80-28, (AD-A091762), November 1980.
10. Yanta, W. J. "A Three-Dimensional Laser Doppler Velocimeter (LDV) for Use in Wind Tunnels." International Congress on Instrumentation in Aerospace Simulation Facilities (ICIASF) '79 Record, Naval Postgraduate School, Monterey, California, September 24-26, 1979, pp. 294-301.
11. Crosswy, F. L. "Particle Size Distributions of Several Commonly Used Seeding Aerosols." Proceedings of Wind Tunnel Seeding Systems for Laser Velocimeters. A workshop held at NASA Langley Research Center, Hampton, VA, March 19-20, 1985. NASA CP-2393, pp. 53-75.
12. May, K. R. "The Collison Nebulizer: Description, Performance and Application." Aerosol Science, Vol. 4, 1973, pp. 235-243.
13. Adams, J. C., Jr. "Eddy Viscosity-Intermittency Factor Approach to Numerical Calculation of Transitional Heating on Sharp Cones in Hypersonic Flow." AEDC-TR-70-210 (AD-714058), November 1970.
14. Adams, J. C., Jr. "Implicit Finite-Difference Analysis of Compressible Laminar, Transitional, and Turbulent Boundary Layers Along the Windward Streamline of a Sharp Cone at Incidence." AEDC-TR-71-235 (AD-734535), December 1971.
15. Schlichting, Herman. Boundary Layer Theory. Translated by Kestin, J., McGraw-Hill Book Company, New York, 1979 (Seventh Edition).
16. McLaughlin, D. K. and Tiederman, W. G. "Biasing Correction for Individual Realization of Laser Anemometer Measurements in Turbulent Flows." Physics of Fluids, Vol. 16, No. 12, December 1973, pp. 2082-2088.
17. Hill, J.A.F., Voisinet, R.L.P., and Wagner, D.A. "Measurements of Surface Roughness Effects on the Heat Transfer to Slender Cones at Mach 10." AIAA Paper No. 80-0345, AIAA 18th Aerospace Sciences Meeting, Pasadena, CA, January 14-16, 1980.



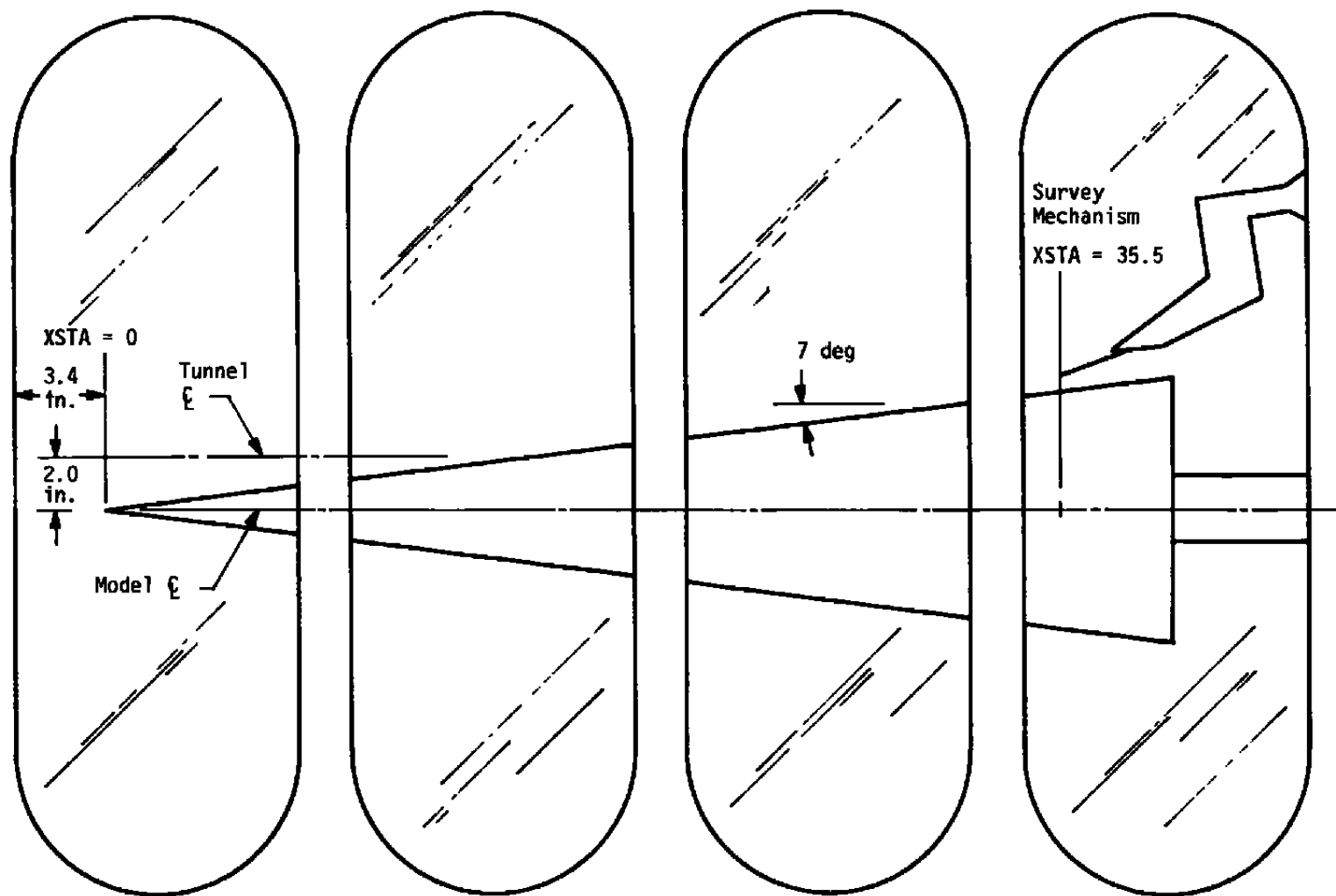
**a. Tunnel assembly**



**b. Tunnel test section**  
**Figure 1. Supersonic Wind Tunnel (A).**



c. Tunnel stilling chamber, nozzle section  
Figure 1. Concluded.



Note: Model axial location is adjustable. (Forward-Most Location Is Shown.)

Figure 2. Tunnel A vertical window panels.

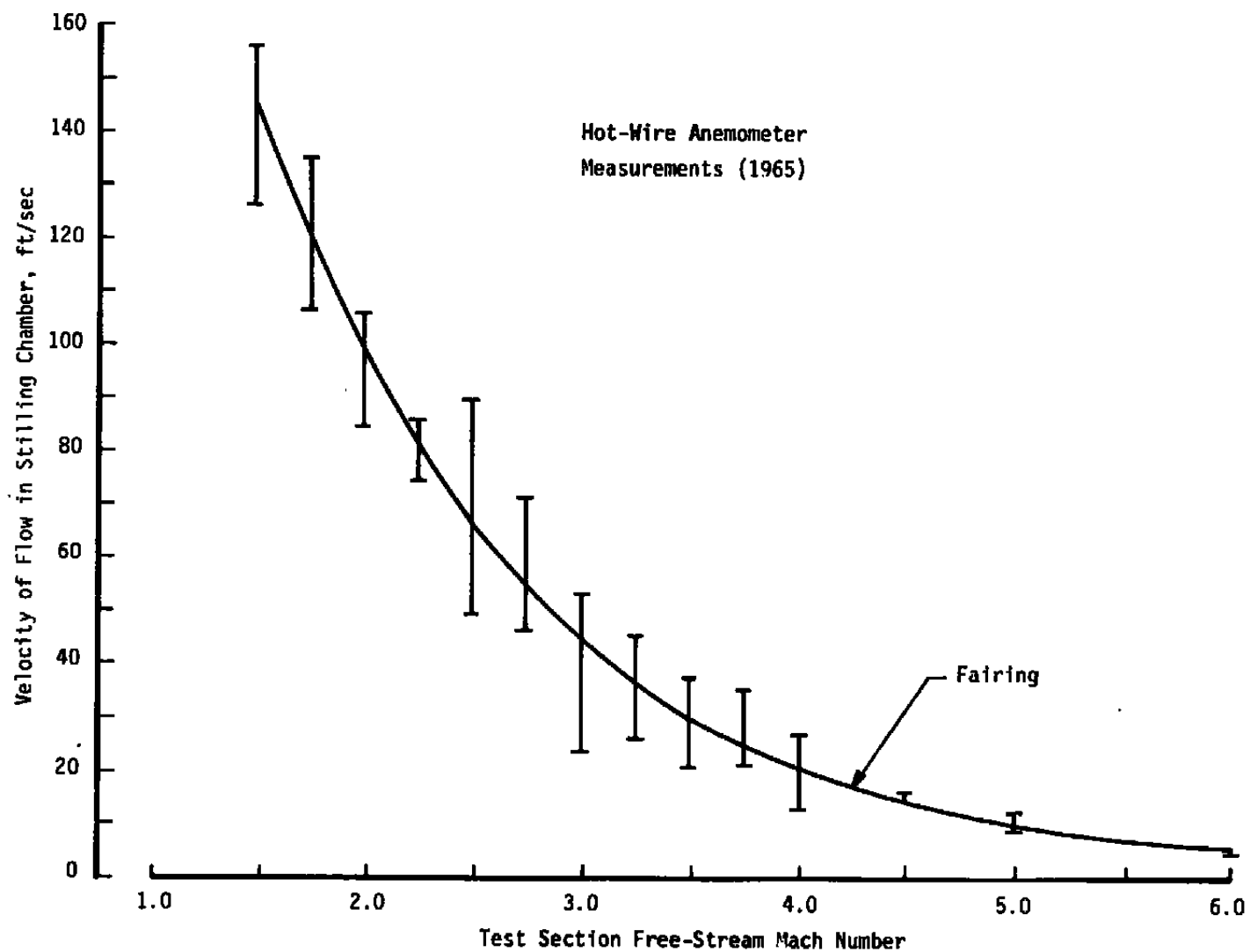


Figure 3. Tunnel A stilling chamber flow velocity at station of seed introduction.

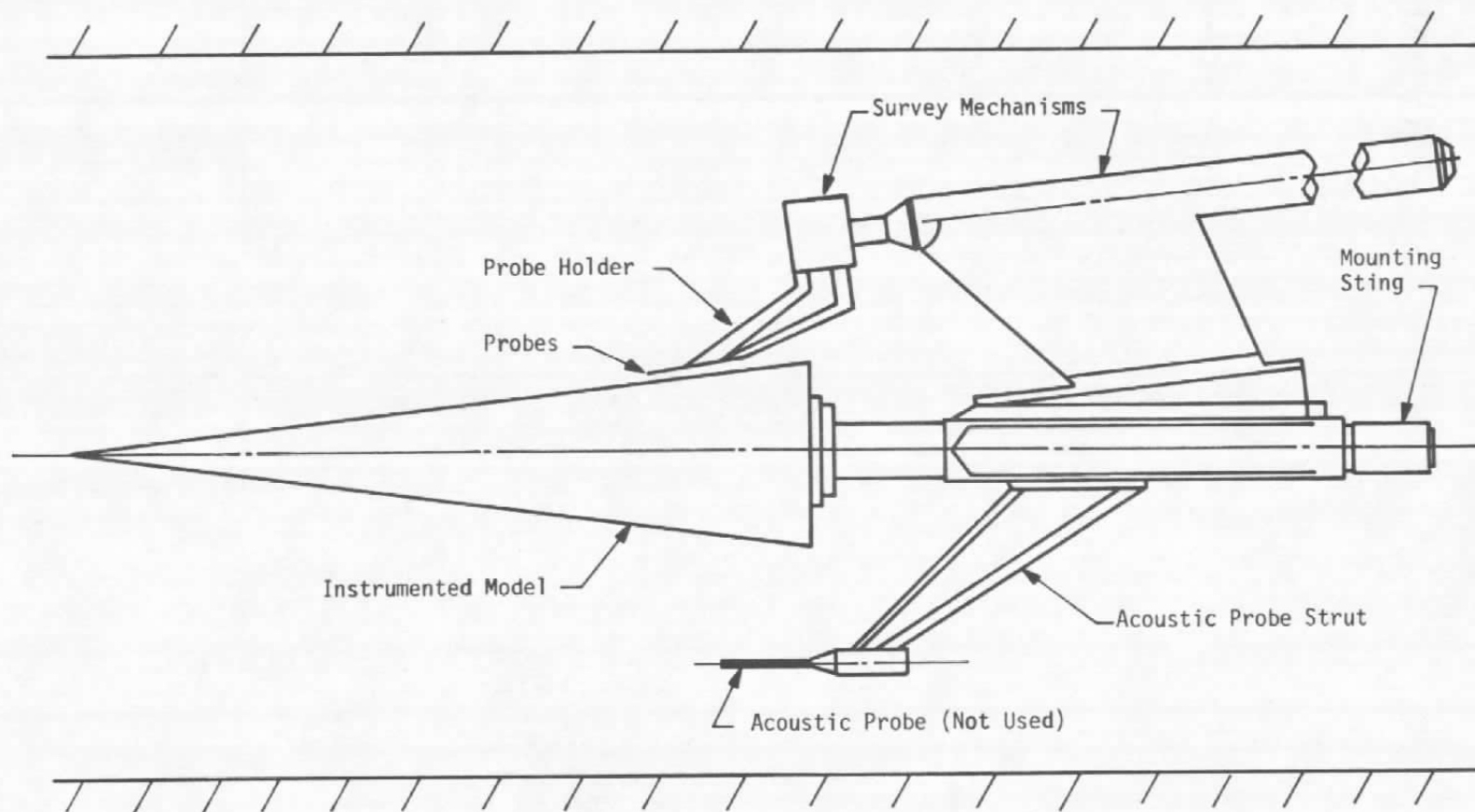
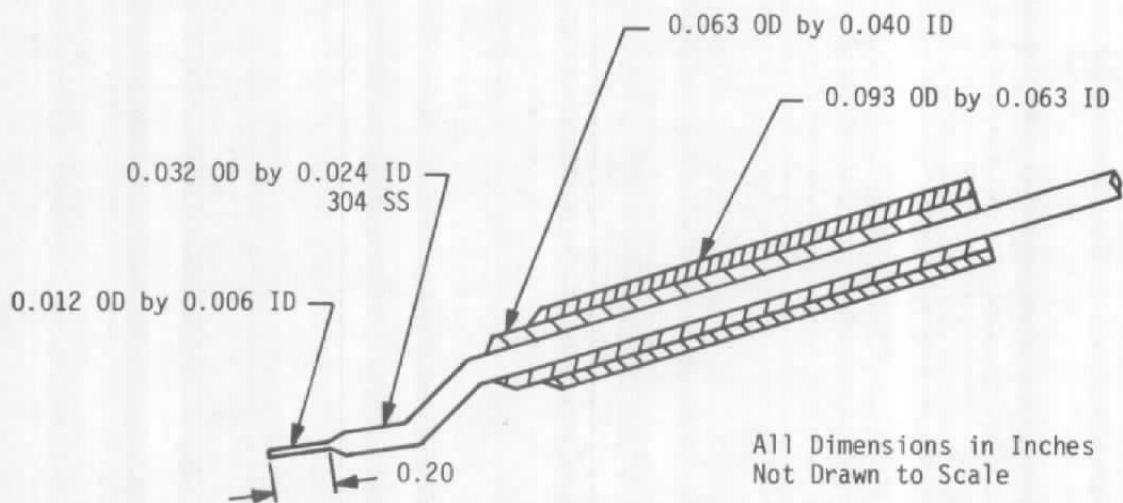
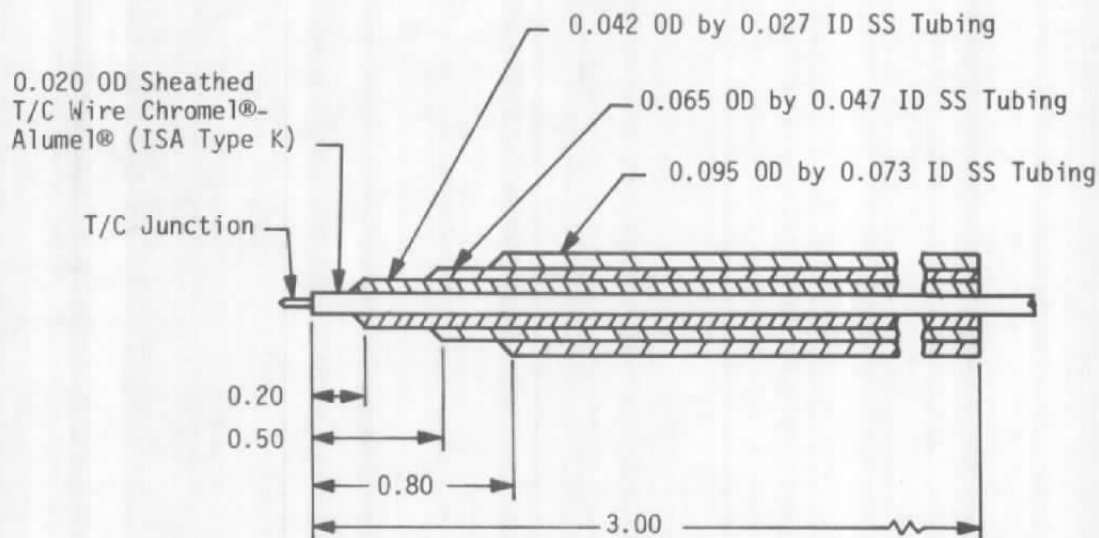


Figure 4. Model and probe systems assembly.



**a. Pitot probe**



**b. Total temperature probe**

**Figure 5. Probe details.**



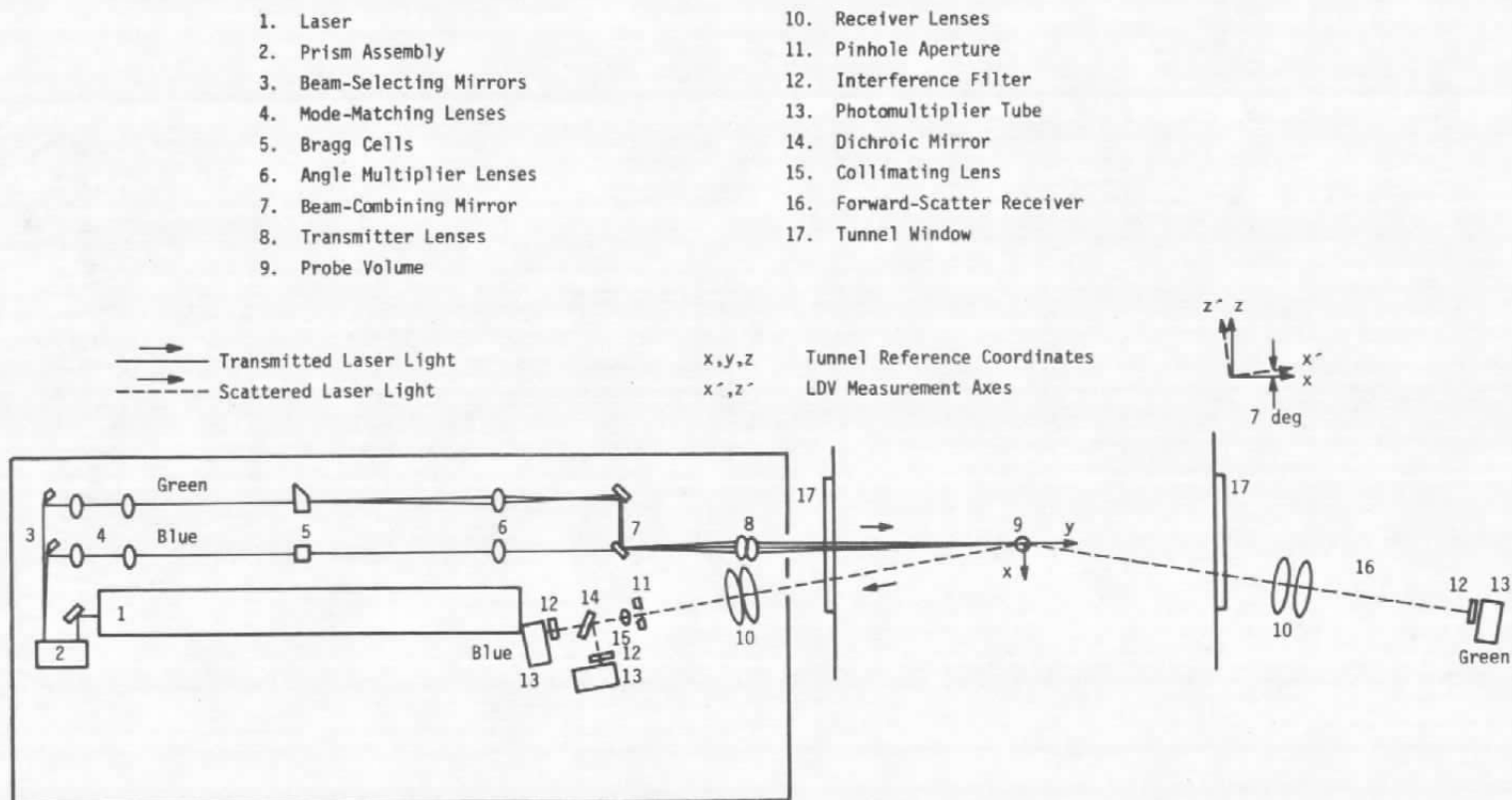
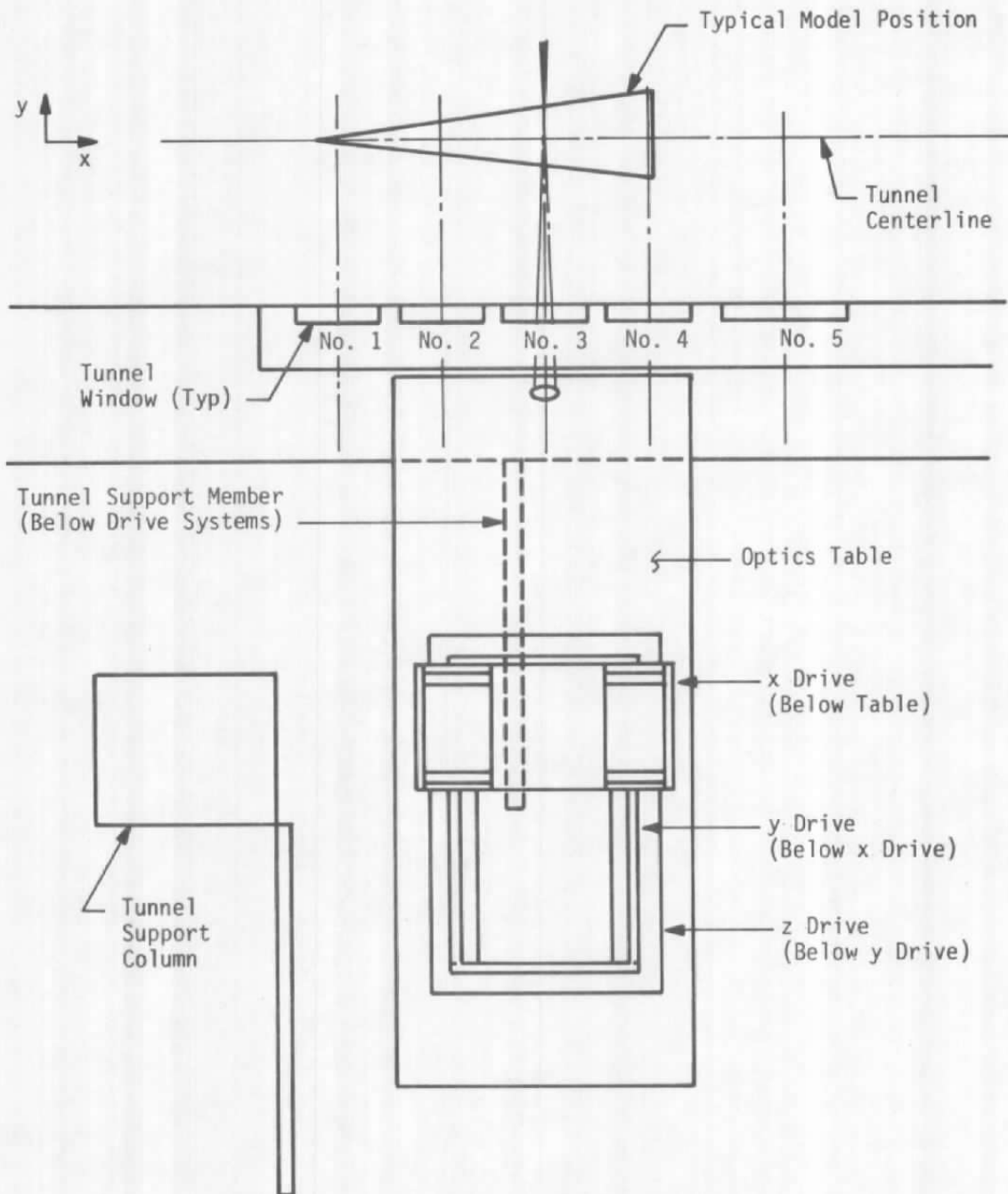
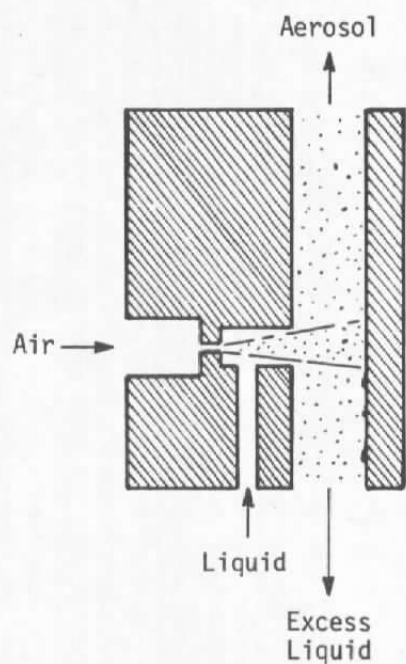


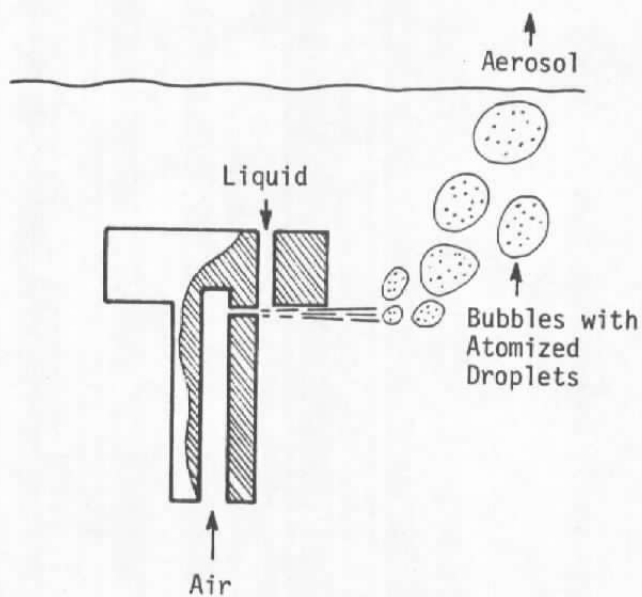
Figure 6. Schematic diagram of laser Doppler velocimeter optical system.



**Figure 7. Tunnel A installation of LDV traversing system.**



**a. Collision nebulizer**



**b. Laskin nozzle**

**Figure 8. Atomizer description.**

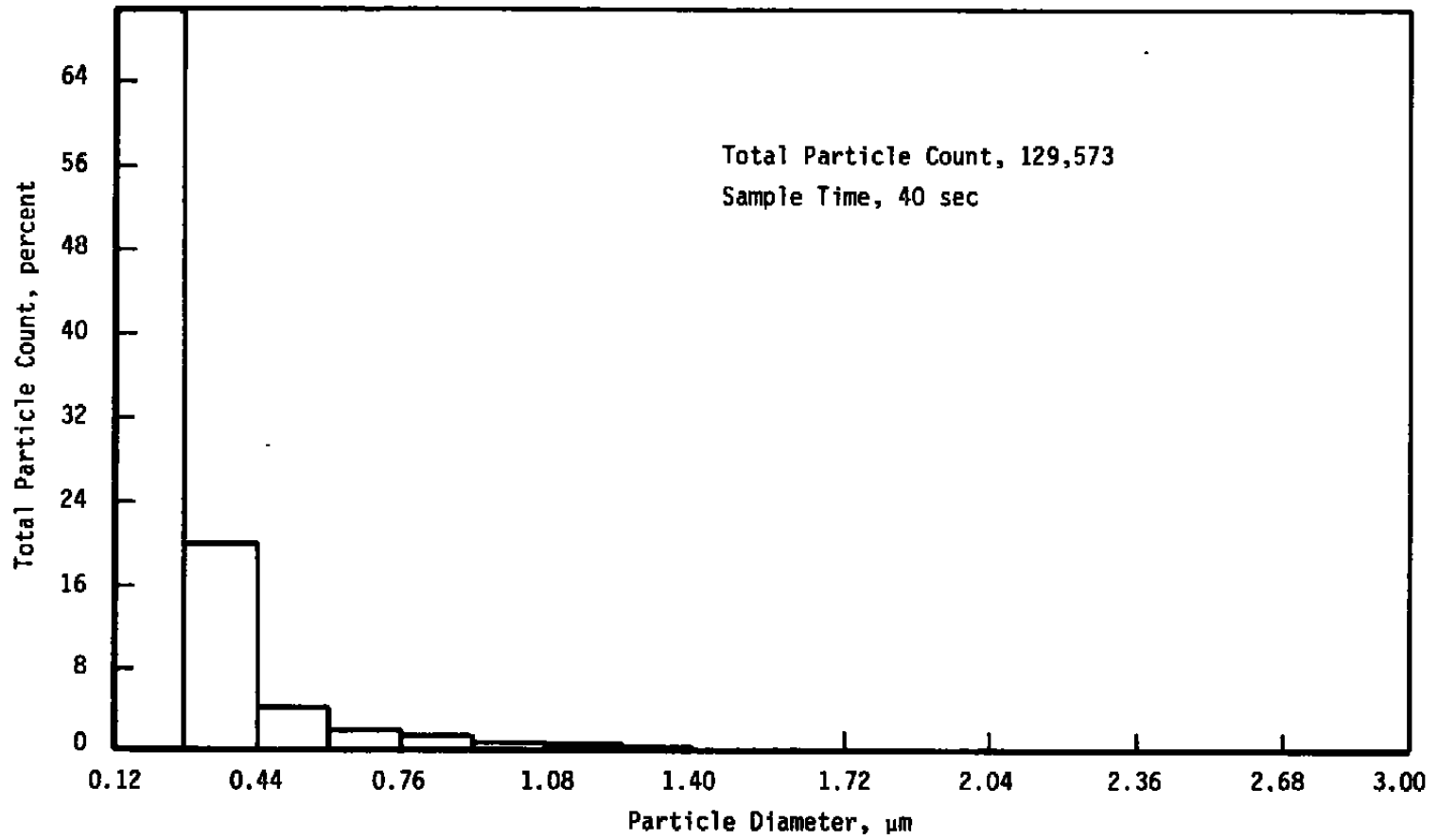


**Figure 9. Particle size distribution for olive-oil droplets produced by the Collison nebulizer.**

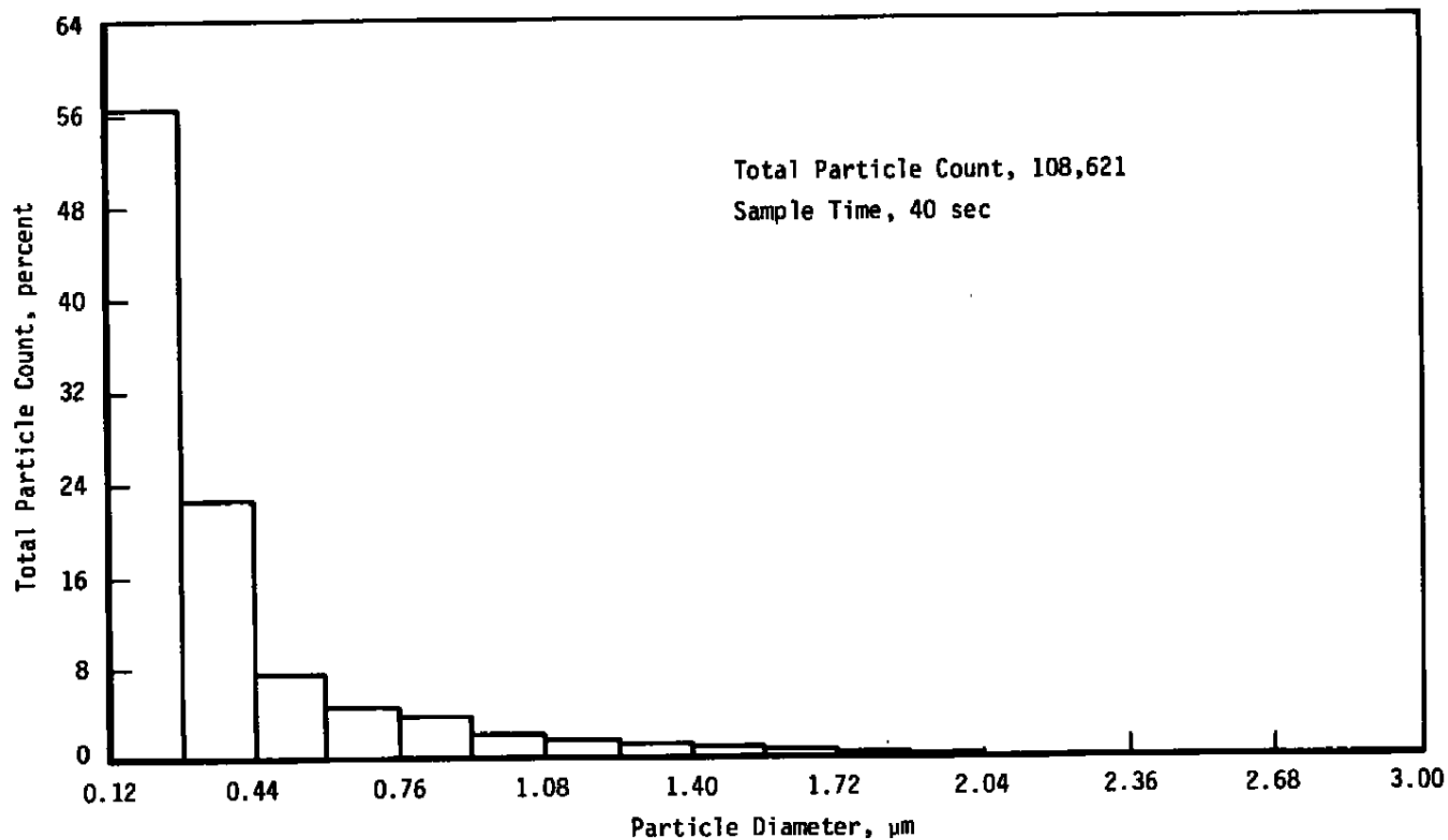


**Figure 10. Particle size distribution for olive-oil droplets produced by the Laskin nozzle.**

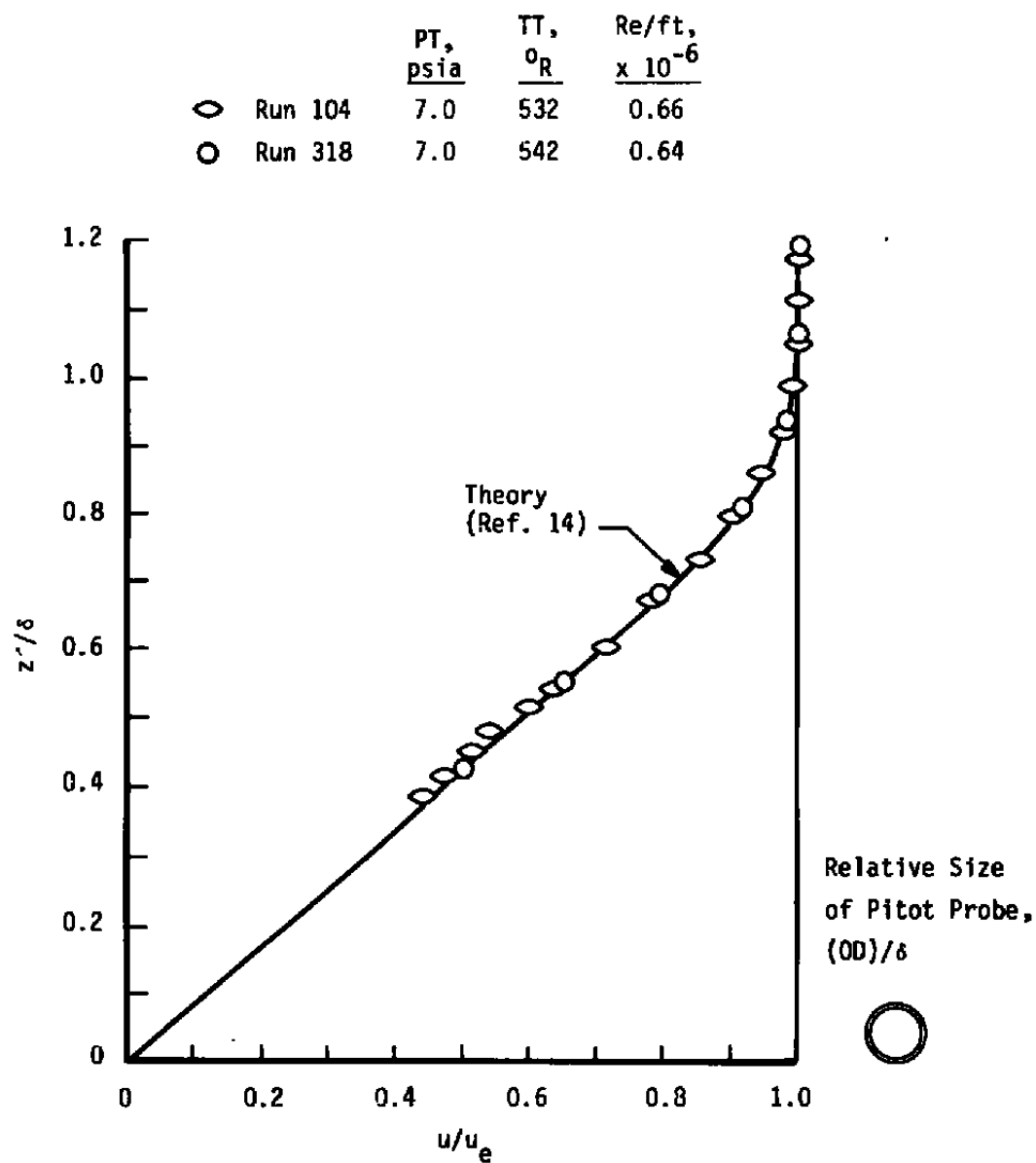


**Figure 11. Laminar boundary-layer velocity profiles obtained using conventional probes.**

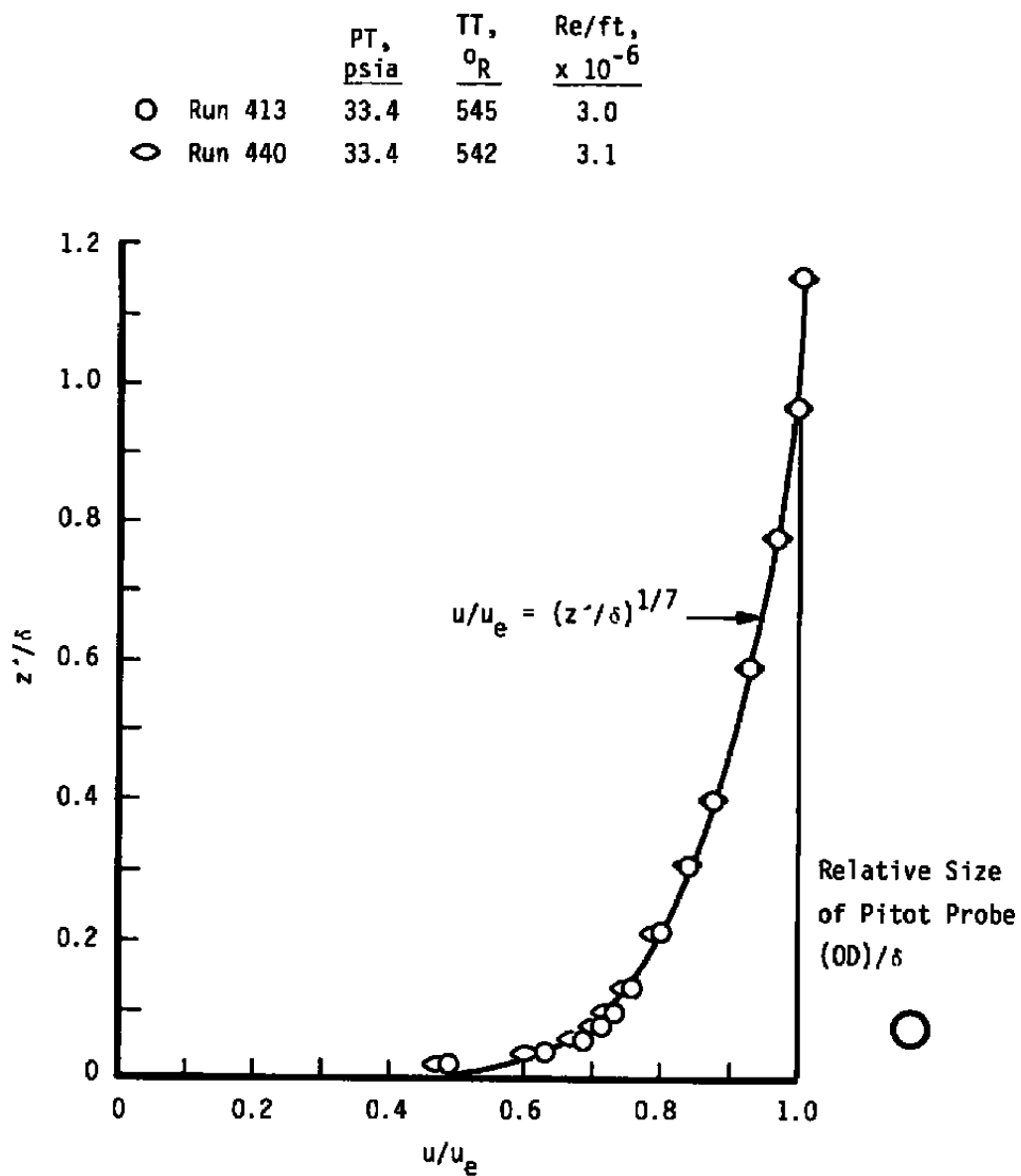


**Figure 12. Turbulent boundary-layer velocity profiles obtained using conventional probes.**

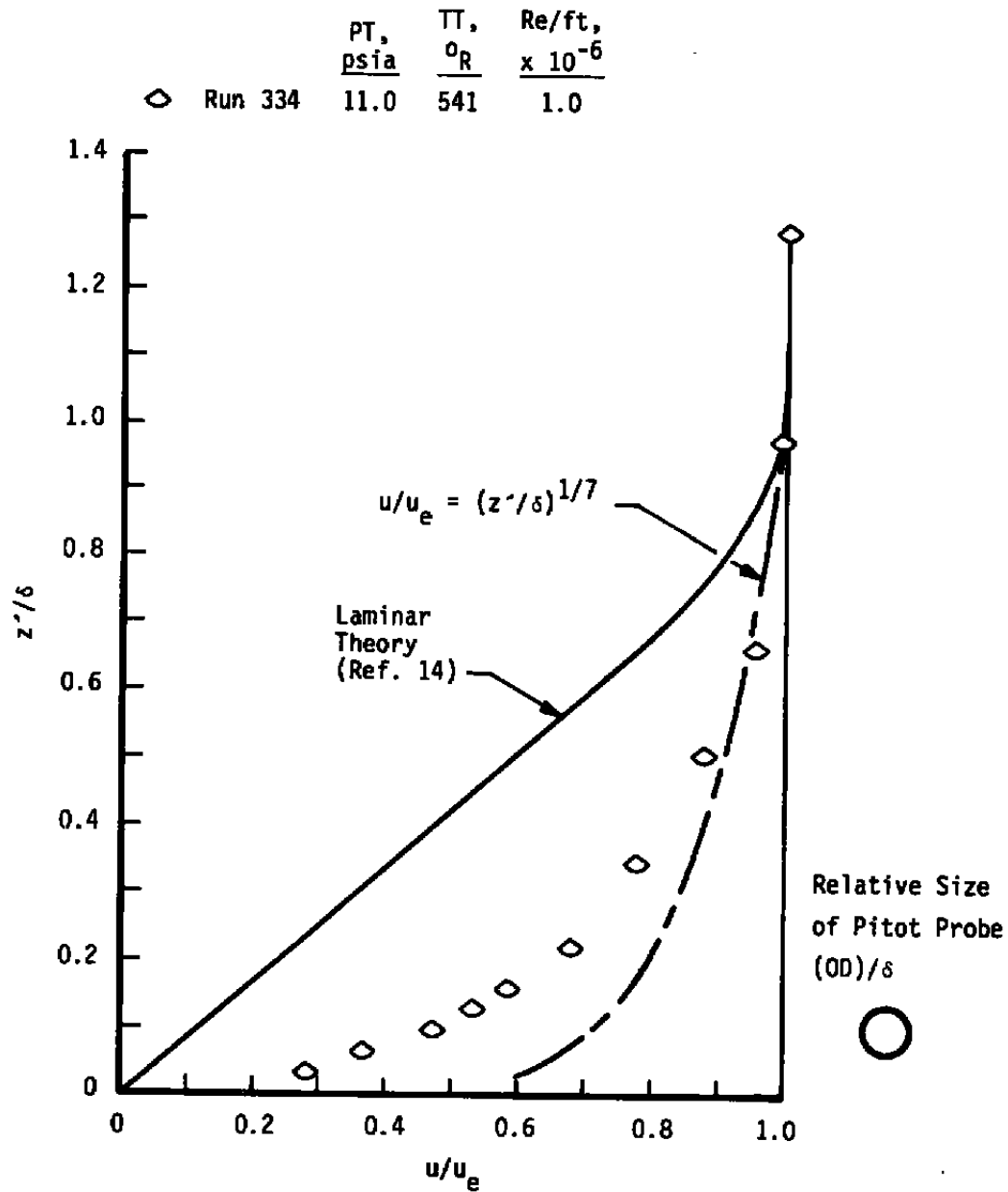


**Figure 13. Transitional boundary-layer velocity profile obtained using conventional probes.**



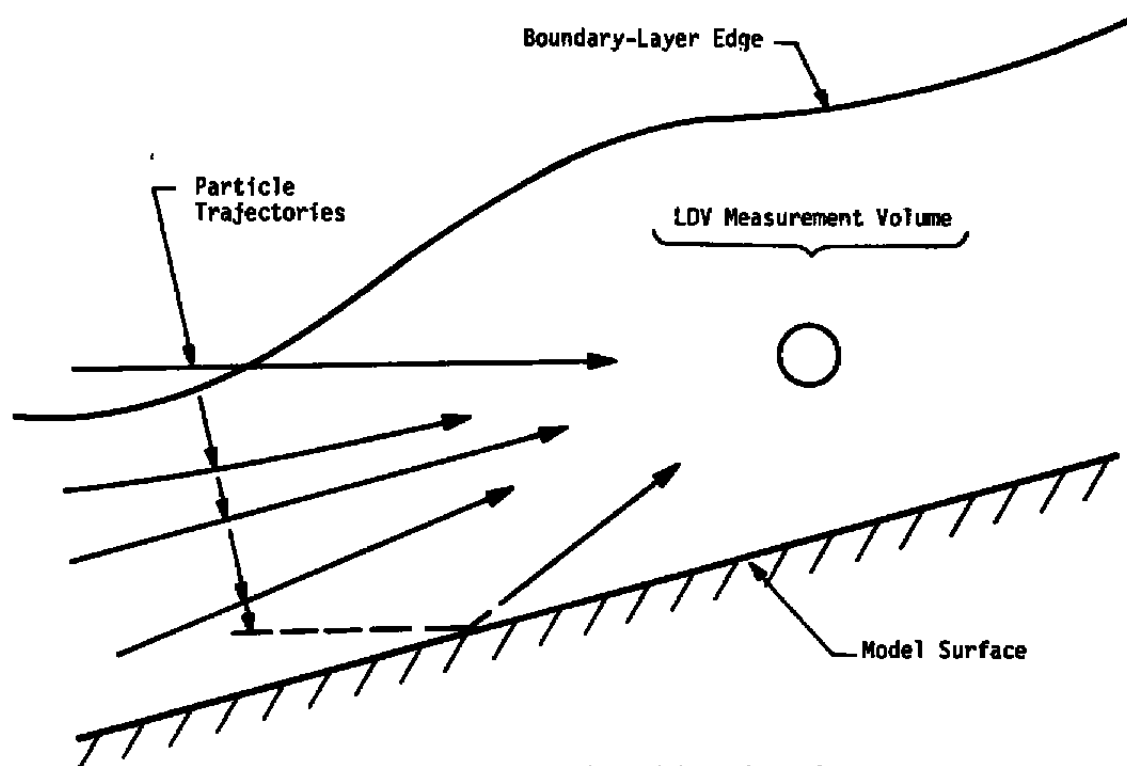


**Figure 14. Concept of particle trajectories.**

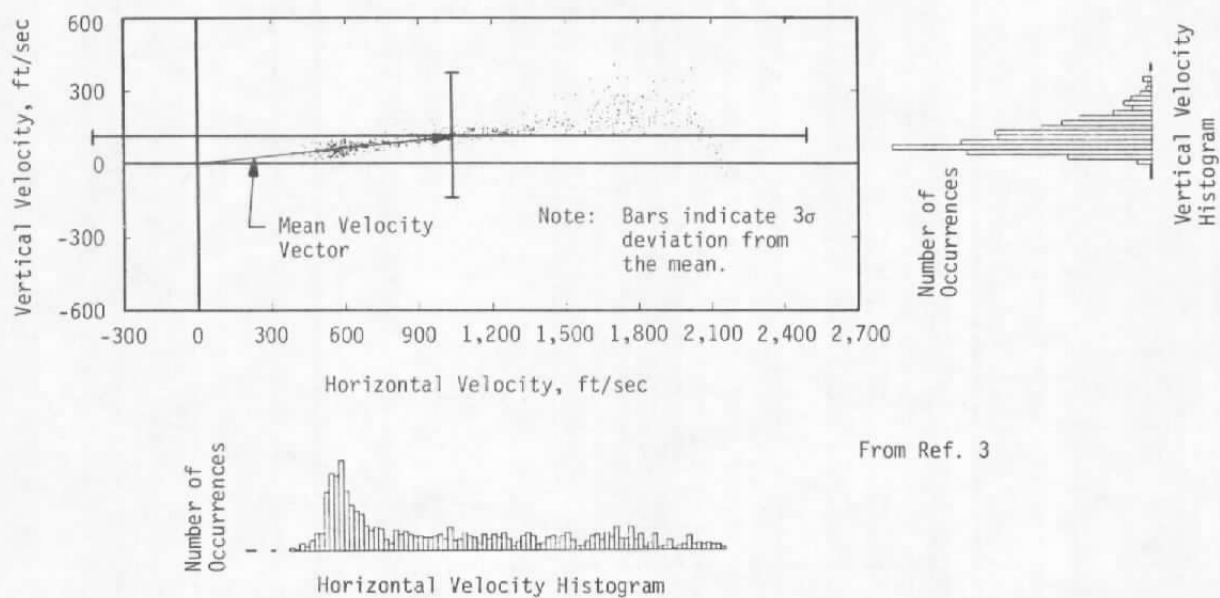


**Figure 15. Simultaneous measurements in the laminar boundary layer.**

	Unedited	Edited
Mean, ft/sec	649.3	150.4
Standard Deviation, ft/sec	613.6	40.5

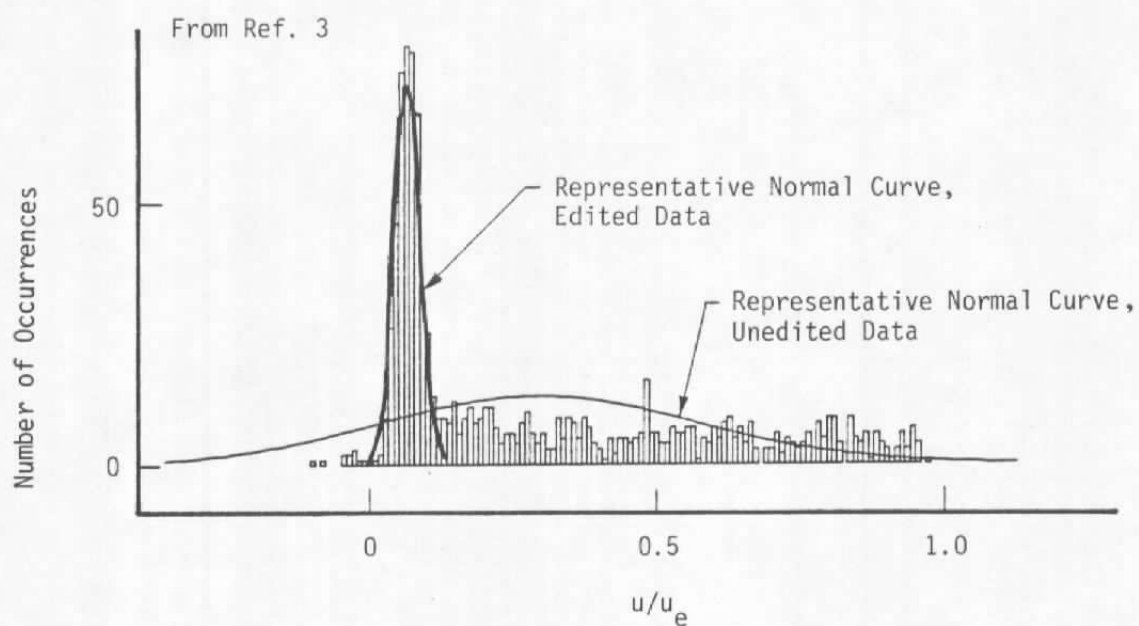
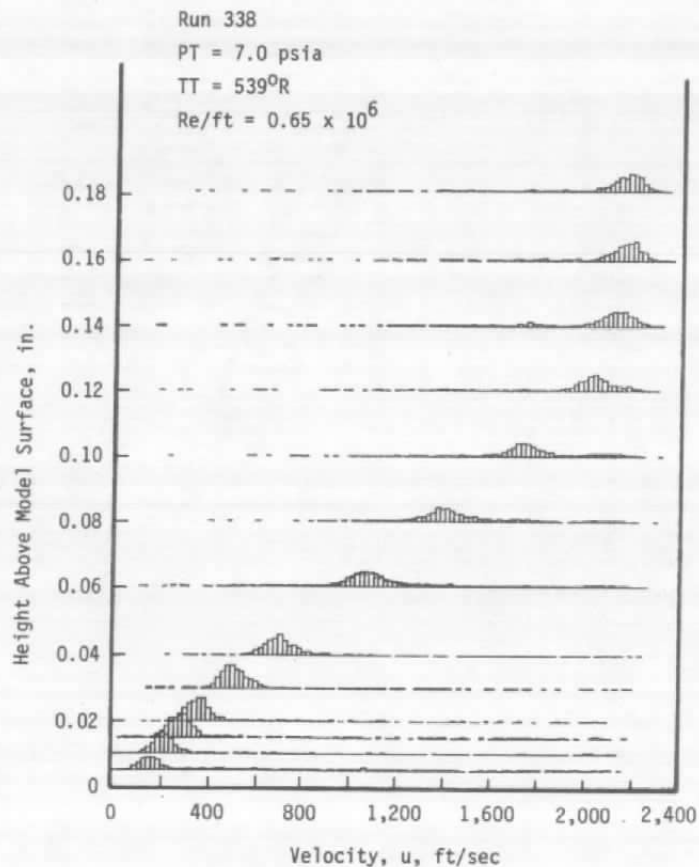
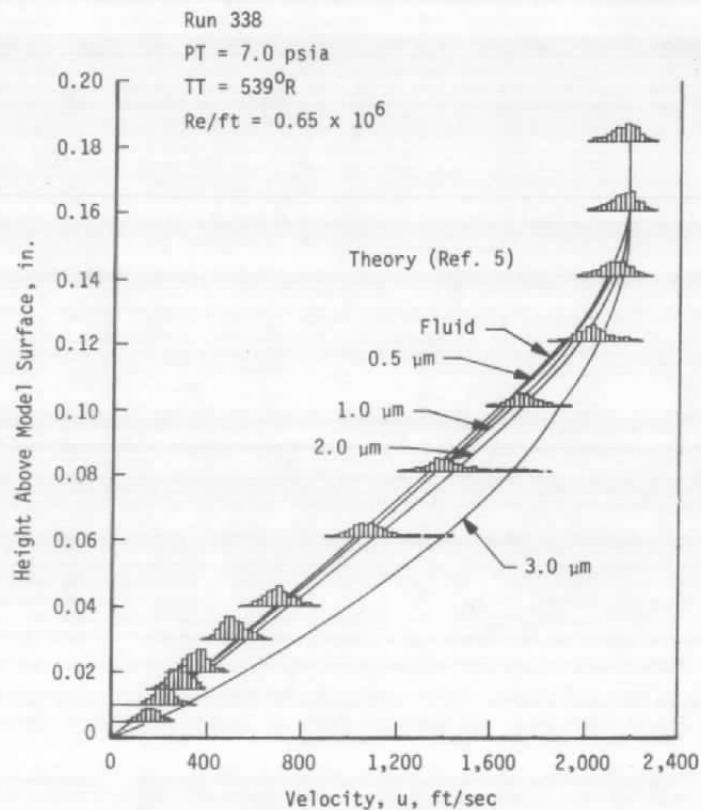


**Figure 16. Example of histogram of measured velocity.**

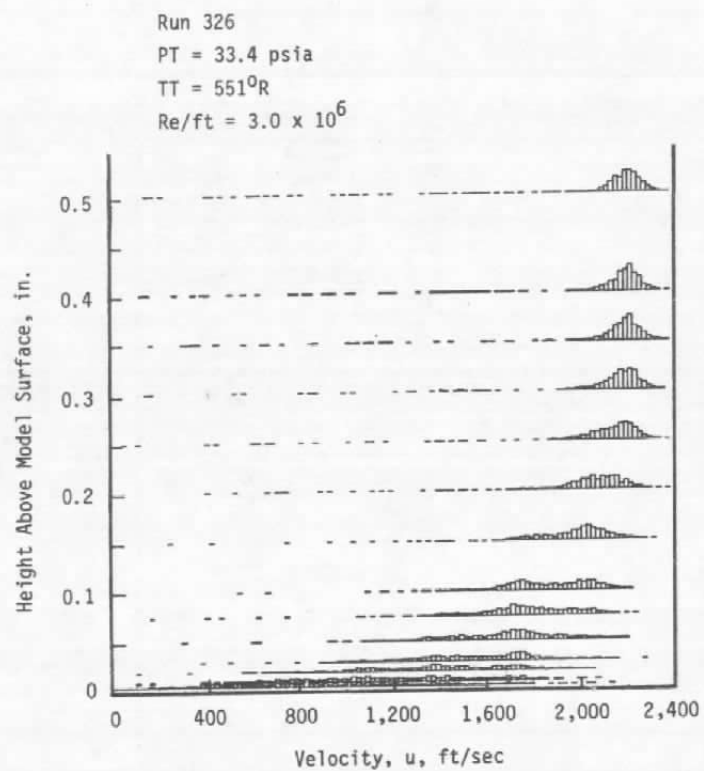


**a. Measured histograms**

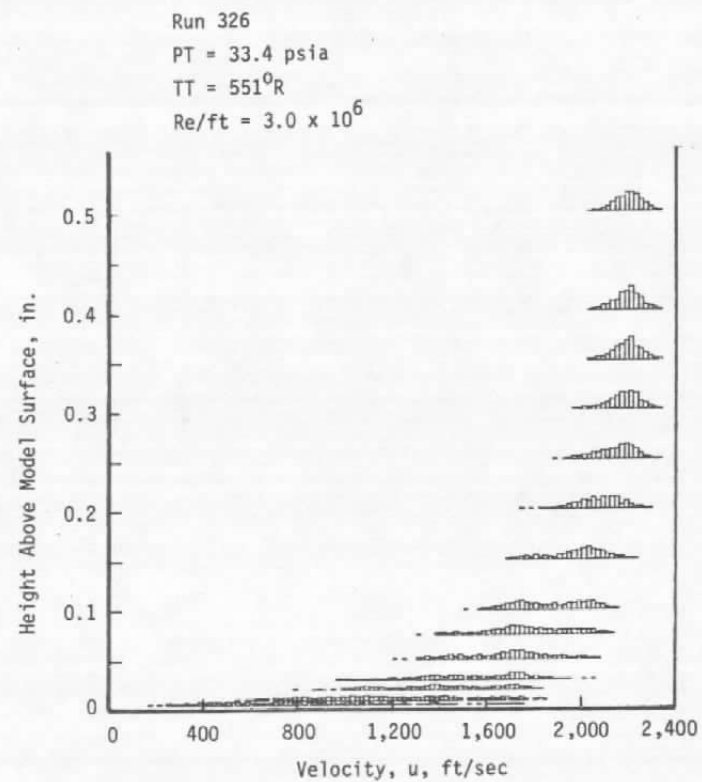


**b. Edited histograms**

**Figure 17. Stacked histograms for laminar boundary layer.**

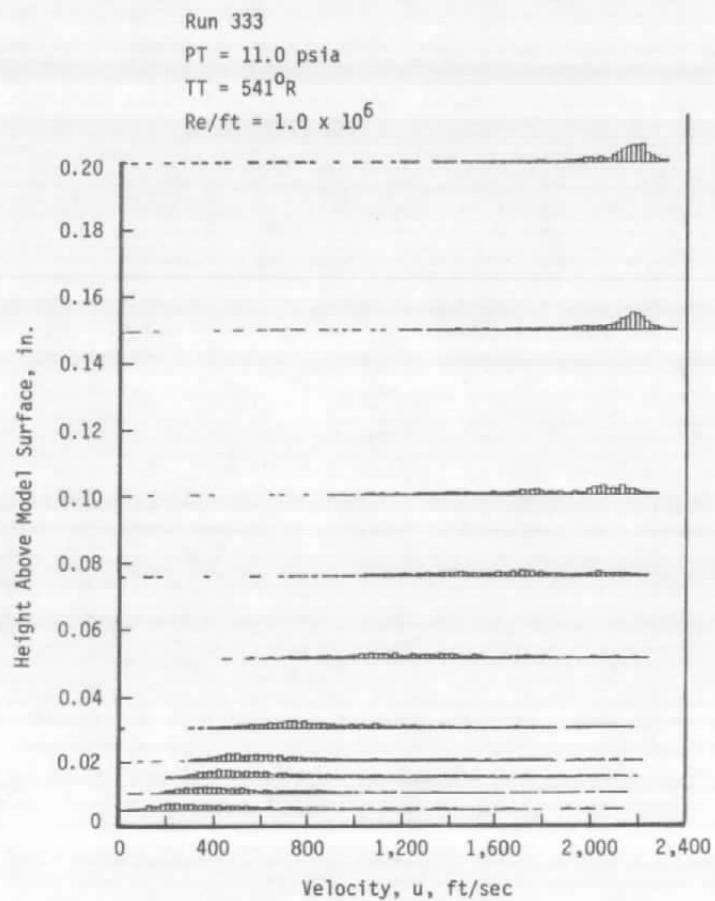


a. Measured histograms

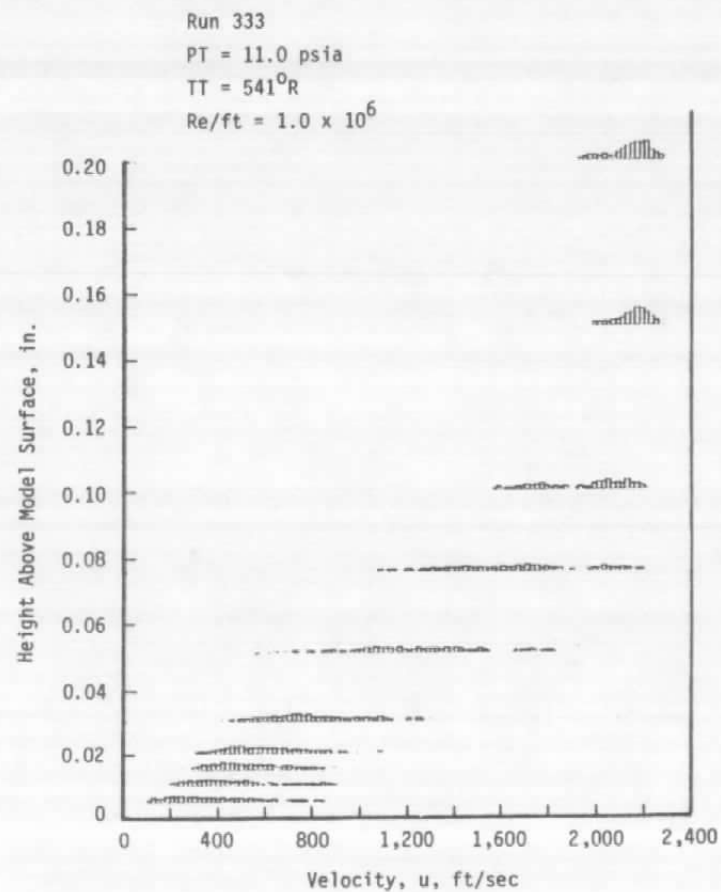


b. Edited histograms

Figure 18. Stacked histograms for turbulent boundary layer.



a. Measured histograms



b. Edited histograms

Figure 19. Stacked histograms for transitional boundary layer.

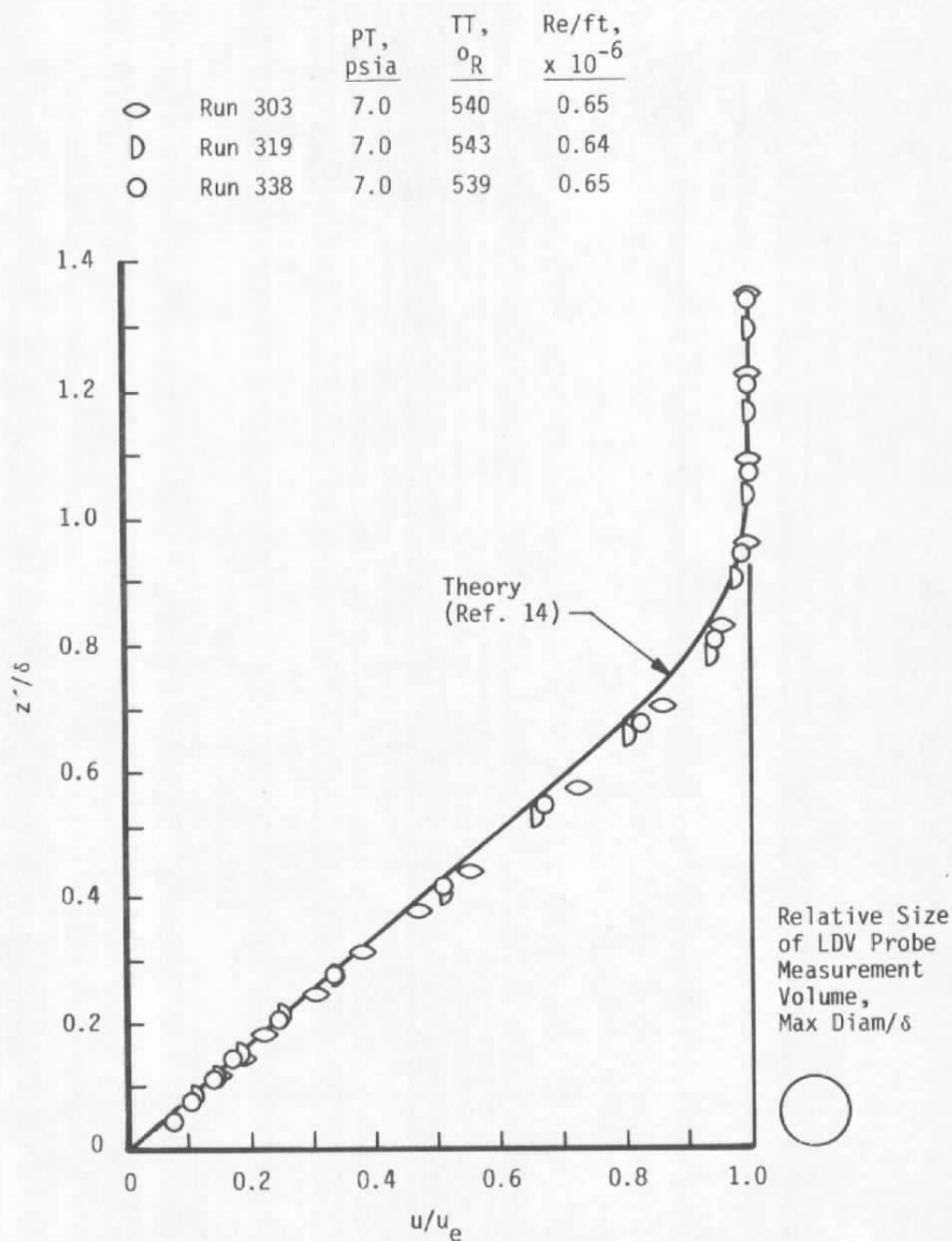


**Figure 20. Laminar boundary-layer velocity profile obtained using LDV techniques.**

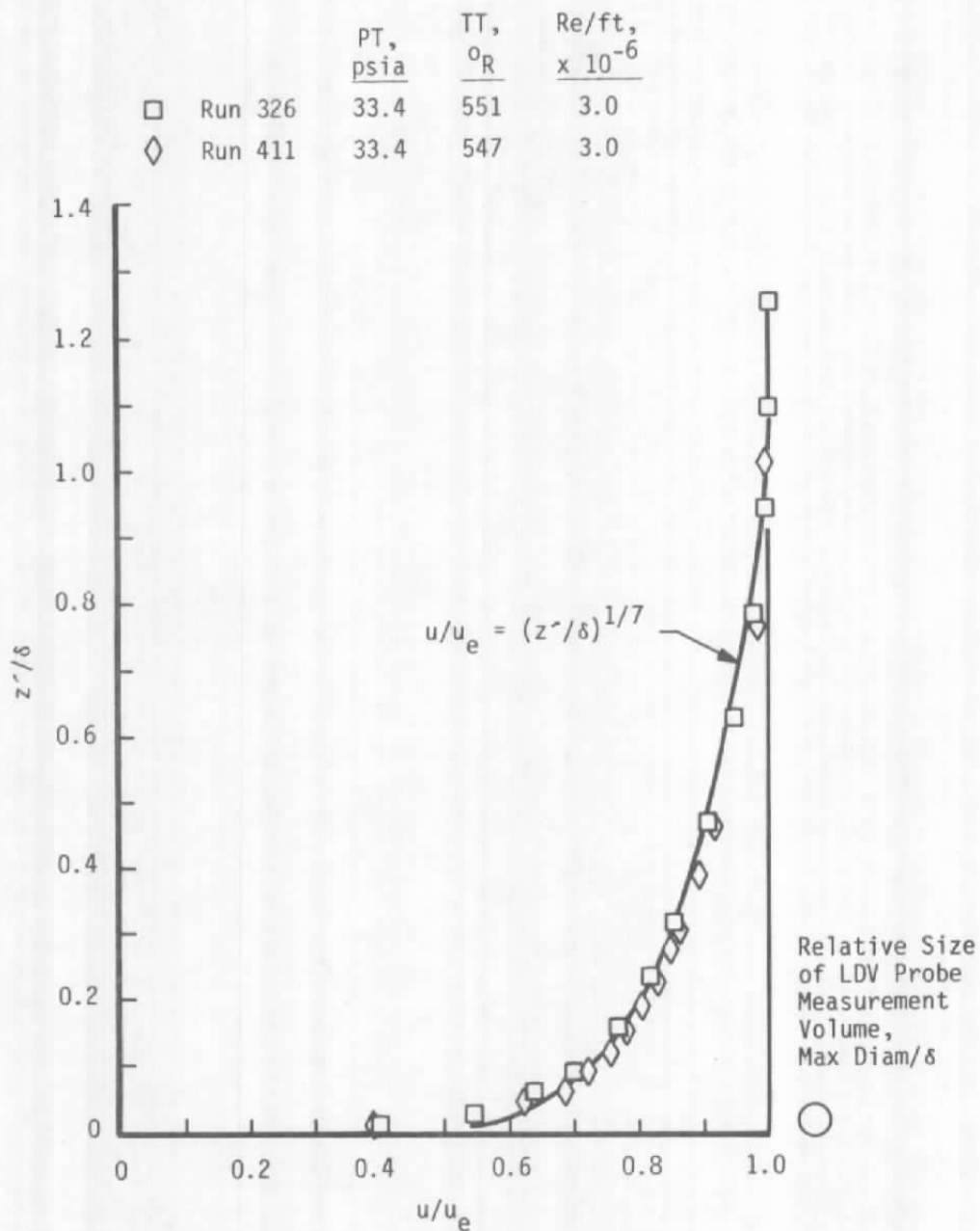


**Figure 21. Turbulent boundary-layer velocity profile obtained using LDV techniques.**



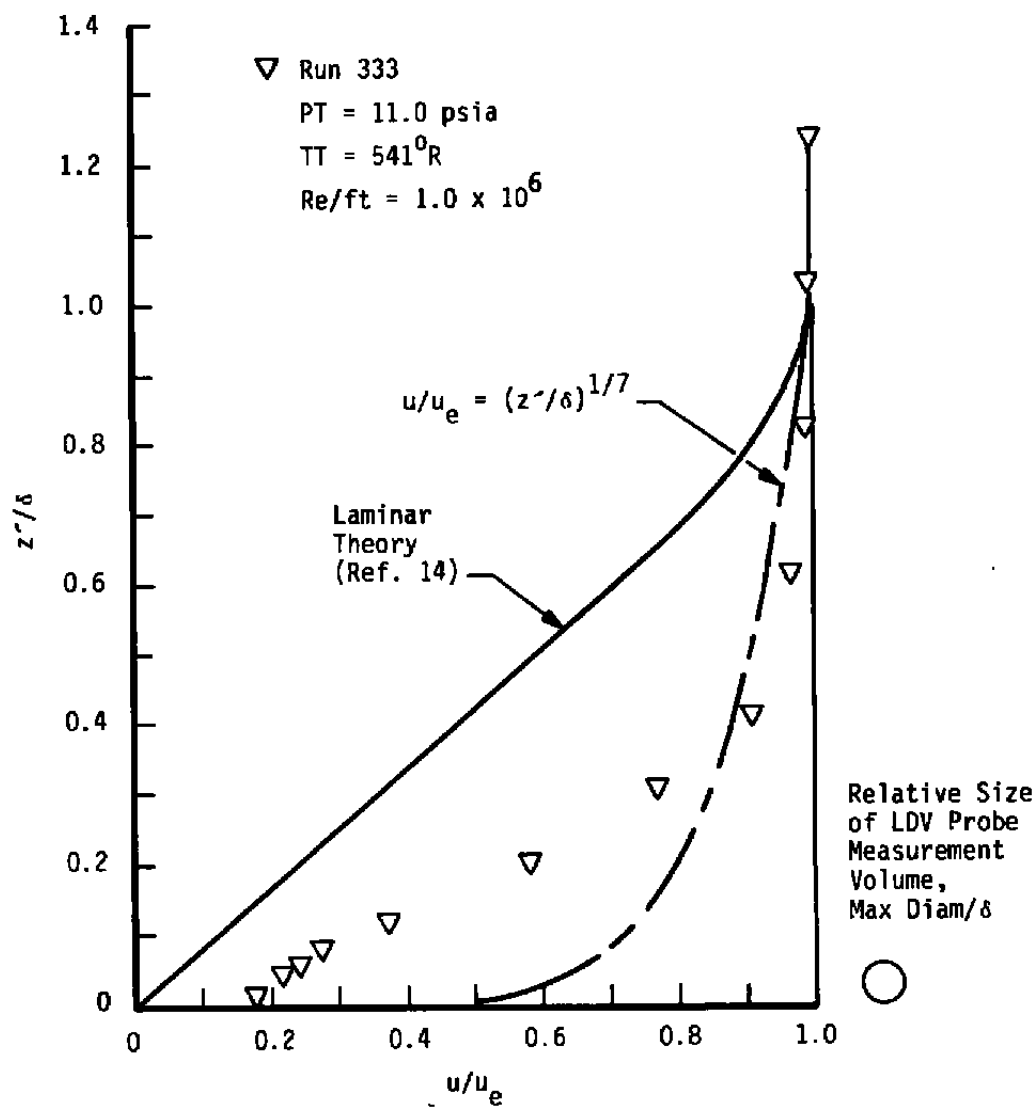


**Figure 22. Transitional boundary-layer velocity profile obtained using LDV techniques.**

	$Re/ft, \times 10^{-6}$	$u_{\tau},$ ft/sec	Run
○	0.65	86	338
△	1.0	98	333
□	3.0	114	326

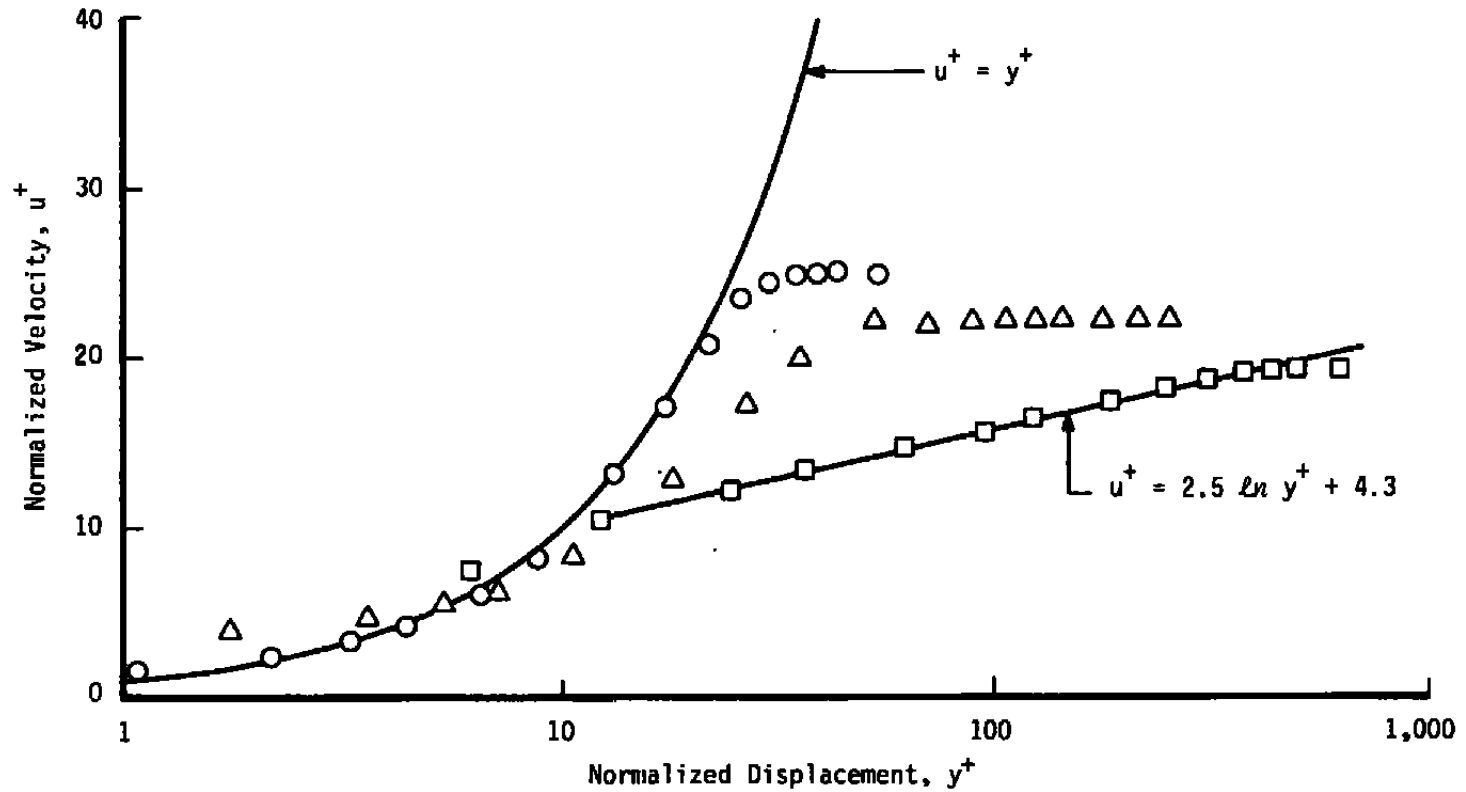
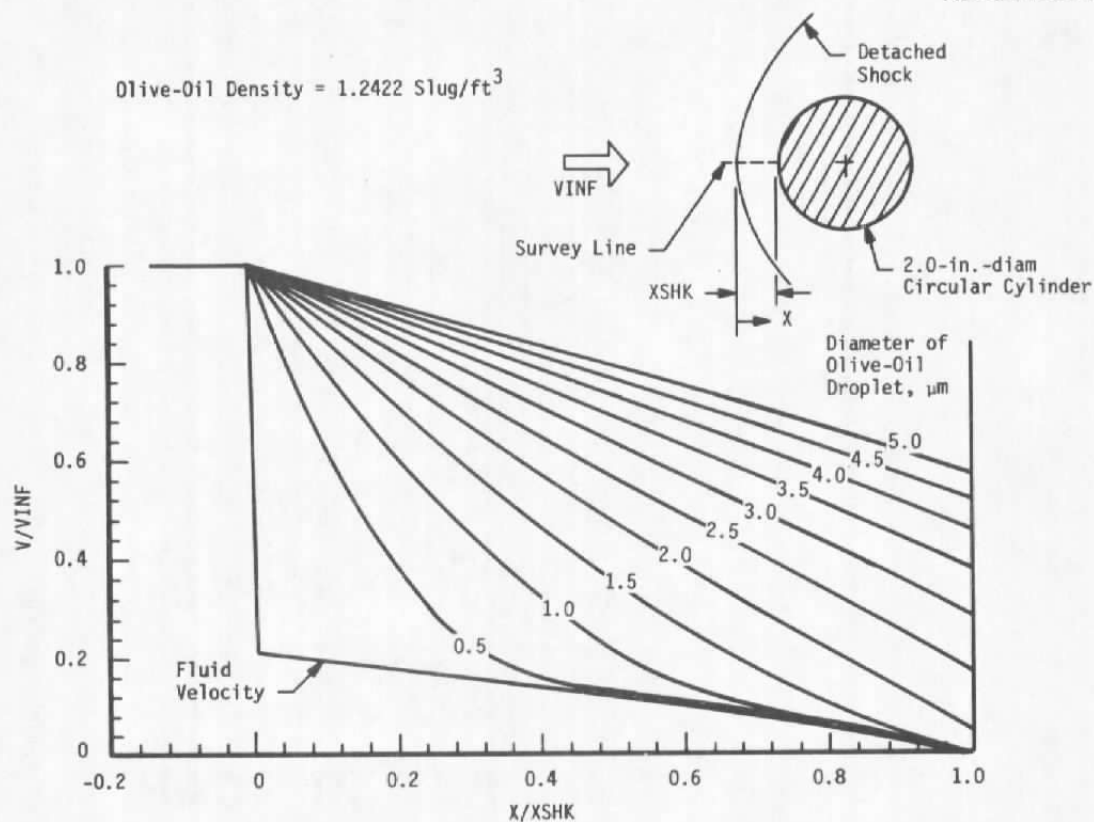
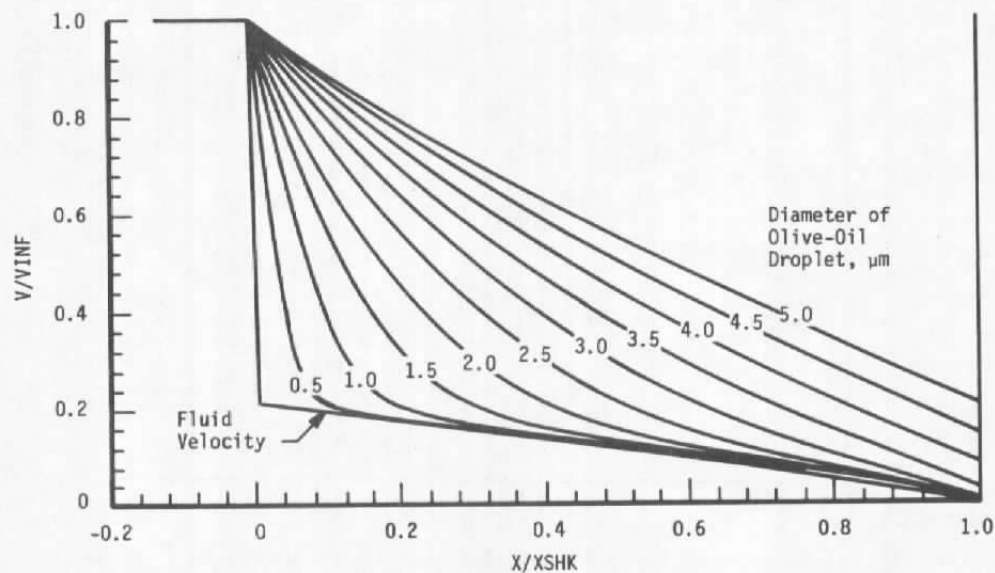
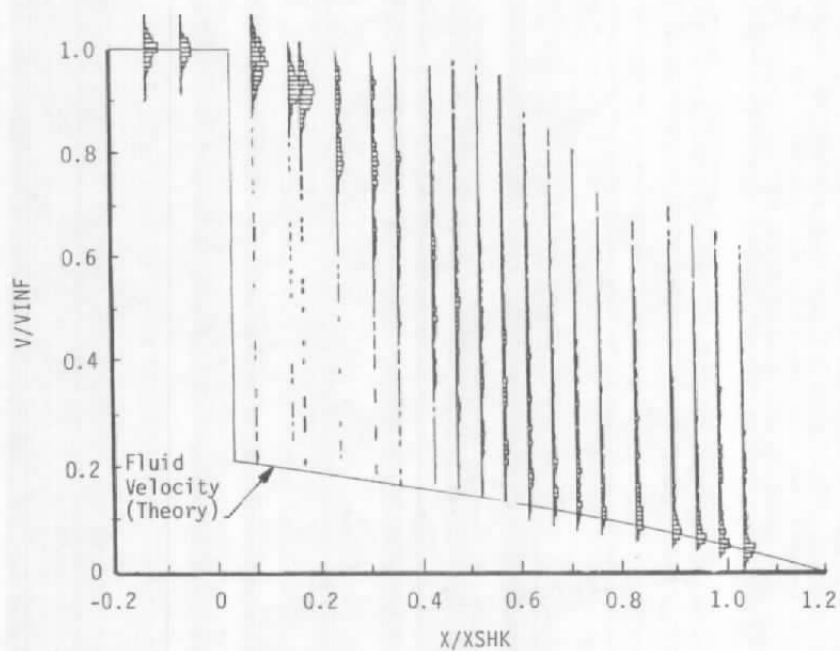
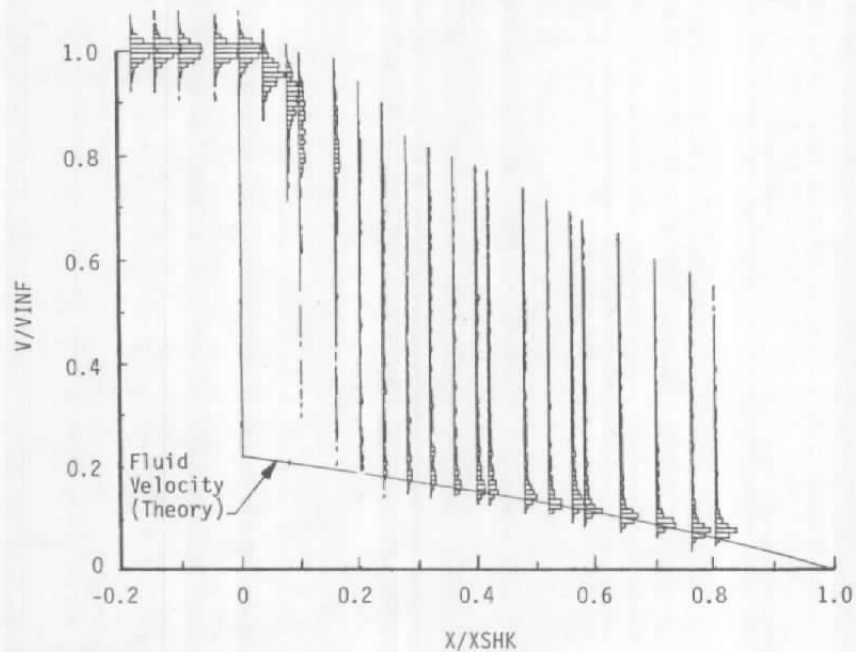


Figure 23. Law-of-the-wall velocity profiles.

a.  $Re/ft = 0.6 \text{ million}$ b.  $Re/ft = 3.0 \text{ million}$ Figure 24. Computed particle response to a normal shock wave,  $M = 4$ .

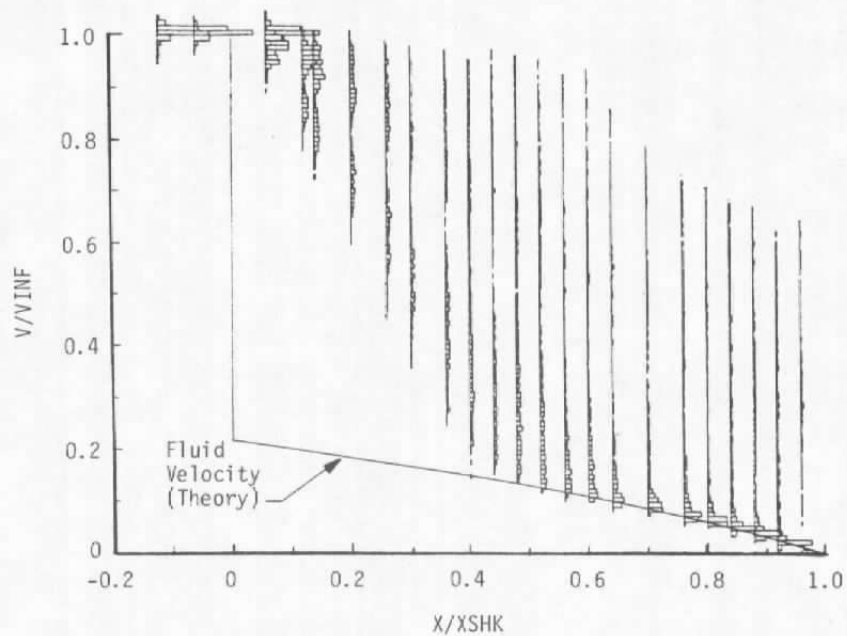


**a.  $Re/ft = 0.65$  million**

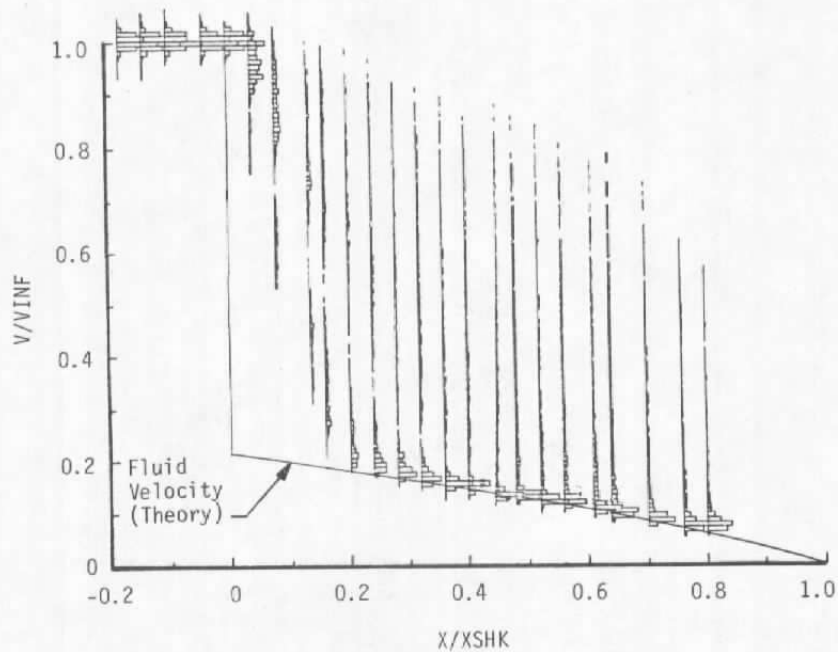


**b.  $Re/ft = 3.1$  million**

**Figure 25. Measured particle response to a normal shock wave, particles from Collision nebulizer, back-scattered light.**

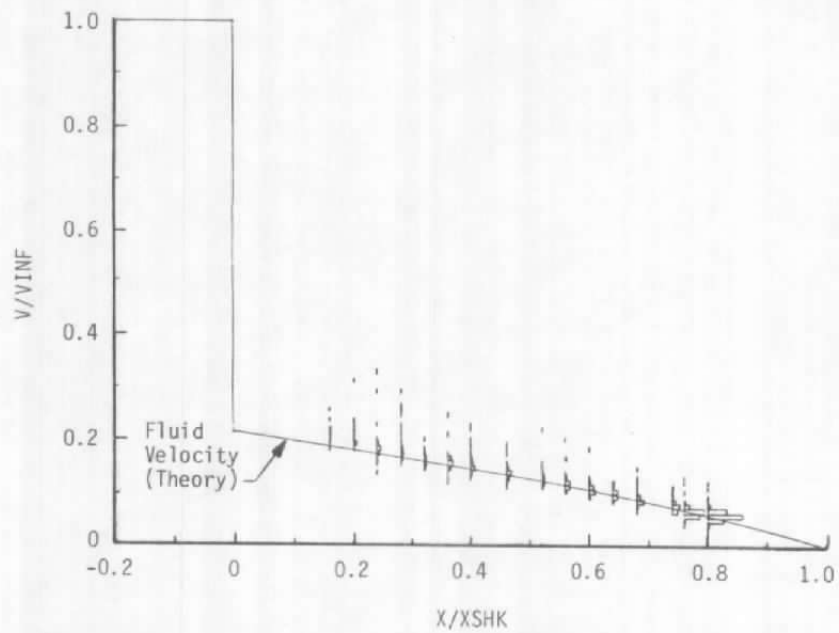


**a.  $Re/ft = 0.65$  million**

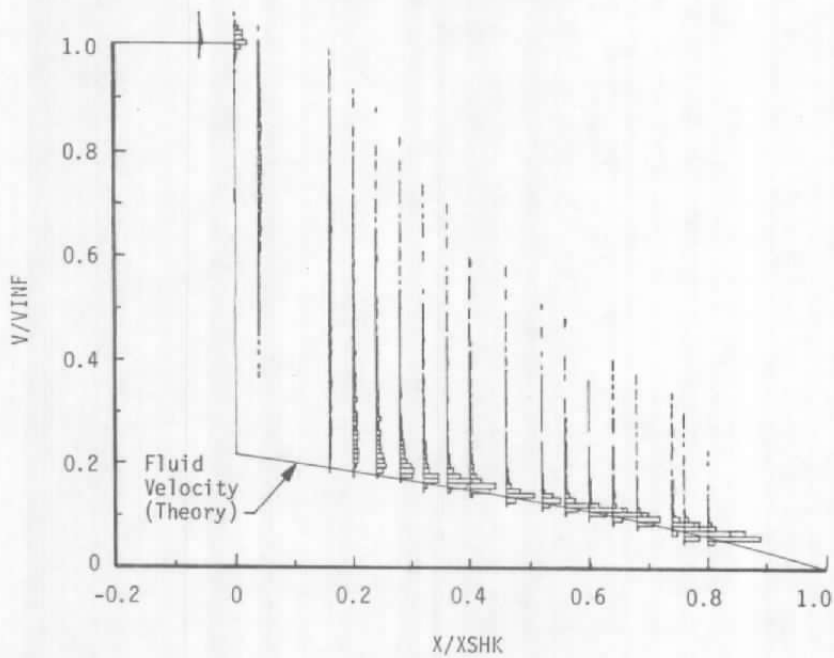


**b.  $Re/ft = 3.1$  million**

**Figure 26. Measured particle response to a normal shock wave, particles from Collison nebulizer, forward-scattered light.**



**a. Back-scattered light**



**b. Forward-scattered light**

**Figure 27. Measured particle response to a normal shock wave, ambient particles,  $Re/ft = 3.1$  million.**

Table 1. Run Summary

Run No.	Flow Field	Survey Technique	Seeder	PT, psia	TT, °R	Re/ft $\times 10^{-6}$	XSTA, in.	Traverse Used
103	Boundary Layer ↓	Probes ↓	---	7.0	540	0.65	35.5 ↓	Probe ↓
104			---	7.0	532	0.66		
318			---	7.0	542	0.65		
327			---	33.4	549	3.0		
334			---	11.0	541	1.0		
413			---	33.4	545	3.0		
430			---	7.0	523	0.68		
440			---	33.4	542	3.1		
105	Boundary Layer ↓	LDV ↓	Laskin	7.0	532	0.66	35.0 ↓	Optics
201			None Collision ↓	7.0	533	0.66		Model
301				7.0	536	0.65		Model
303				7.0	540	0.65		Model
319				7.0	543	0.64		Optics
326				33.4	551	3.0		Optics
333				11.0	541	1.0		Optics
338				7.0	539	0.65		Optics
411				33.4	547	3.0		Model
427				7.0	524	0.68		Optics
429				7.0	523	0.68		Optics
114	Shock Layer ↓	LDV ↓	Laskin	7.0	530	0.66	---	Model ↓
302			Collision	7.0	536	0.65	---	
414				33.4	543	3.1	---	
415			None	33.4	543	3.1	---	

# **NOMENCLATURE**

<b>M</b>	Free-stream Mach number
<b>PT</b>	Tunnel stilling chamber pressure, psia
<b>Re/ft</b>	Free-stream unit Reynolds number, $\text{ft}^{-1}$
<b>RN</b>	Radius of model nose, in.
<b>TT</b>	Tunnel stilling chamber temperature, °R
<b>u</b>	Local velocity component parallel to model surface, ft/sec
<b><math>u_\tau</math></b>	Local surface shear velocity, $\tau_w / \rho_w$ , ft/sec
<b><math>u^+</math></b>	Normalized velocity, $u/u_\tau$
<b>V</b>	Particle velocity, ft/sec
<b>VINF</b>	Particle velocity upstream of normal shock wave, ft/sec
<b>X</b>	Horizontal distance downstream of normal shock wave, in.
<b>XSHK</b>	Horizontal standoff distance of normal shock wave, in.
<b>XSTA</b>	Model axial location of surface station, measured from virtual apex, in.
<b>x, y, z</b>	Tunnel rectangular coordinates, in.
<b><math>x', z'</math></b>	Coordinates measured parallel and normal to model surface, respectively, in.
<b><math>y^+</math></b>	Normalized displacement, $z' u_\tau / \nu_w$ , in.
<b><math>\delta</math></b>	Boundary-layer total thickness, in., $z = \delta$ for $u/u_e = 0.995$



$\mu$	Viscosity, lbf-sec/ft <sup>2</sup>
$\nu$	Kinematic viscosity, $\mu/\rho$ , ft <sup>2</sup> /sec
$\rho$	Density lbf/ft <sup>3</sup>
$\sigma$	Standard deviation of velocity, ft/sec
$\tau_w$	Surface shear force, lbf/ft <sup>2</sup>

**Subscripts**

e	Boundary-layer edge value
w	Wall value